EUROPEAN MECHANICAL SCIENCE

2018

VOLUME
02

ISSUE
04

Editor in Chief: M. Ozcanli

EUROPEAN MECHANICAL SCIENCE

Indexed / Abstracted in:

CrossRef, Index Copernicus, Journal Factor, Rootindexing, ResearchBip, JournalFactor, JIFACTOR, Google Scholar, I2OR, Cosmos Impact Factor, International Innovative Journal Impact Factor (IIJIF), Scientific Indexing Services, InfoBase Index, Scientific Journal Impact Factor

Aims and Scopes

European Mechanical Science (EMS) is an international, peer reviewed journal which publishes full length original research papers, reviews related to all areas of Mechanical Engineering such as: Solid Mechanics, Materials Engineering, Automotive Engineering, Fluid Mechanics, Thermal Engineering, Engine and Power Engineering, Dynamics & Control, Robotics & Mechatronics, Transportation Engineering, Computational Mechanics, Design, Systems, Manufacturing, Bio-Medical Engineering; Process Engineering, Aerospace Engineering. No charges are required from the Authors to publish the articles.EMS is a quarterly published journal operating an online submission and peer review system. It allows authors to submit articles online and track their progress via its web interface.

http://dergipark.gov.tr/ems

Contents

EUROPEAN MECHANICAL SCIENCE
e-ISSN: 2587-1110

Research Paper

Out-of-Plane Vibration Analysis of Multiple-Stepped Circular Beam

Timuçin Alp Aslan[1*], Beytullah Temel[2], Ahmad Reshad Noori[3]

[1] Çukurova University, Adana, Turkey, taslan@cu.edu.tr
[2] Çukurova University, Adana, Turkey, btemel@cu.edu.tr
[3]Çukurova University, Adana, Turkey, a.reshadnoori@yahoo.com.tr
ORCID: T.A. Aslan (0000-0002-7558-3568), B. Temel (0000-0002-1673-280X), A.R. Noori (0000-0001-6232-6303)

Abstract

Stepped circular beams are widely used in various engineering fields. Thus, studying the free vibration characteristics of those structures is an essential subject of research. The unified approach of the Complementary Functions Method (CFM) and the Laplace transform is employed in this paper to examine the out-of-plane free vibration analysis of the circular Timoshenko beams with multiple stepped cross-sections. The proposed procedure can be used to investigate the natural frequencies of circular rods consisting of an arbitrary number of steps through the curvature. The material of the beam is considered to be isotropic, homogeneous and elastic. By considering the effects of shear deformation and rotary inertia, the equations of motion of the circular beam are introduced. Obtained equations are transformed to the Laplace domain and solved numerically by the CFM. Comparisons of the results with those of ANSYS show that the suggested scheme is applicable and of high precision for out-of-plane free vibration analysis of multi-stepped circular beams.

Keywords: Out-of-plane free vibration; Multi-stepped circular beam; Laplace transform.

INTRODUCTION

Due to their wide practical applications in civil and mechanical engineering, curved beams have attracted the attention of many researchers. In-plane and out-of-plane free vibrations of curved beams with variable cross-sections was studied by Kawakami et al. [1] by applying the Green function. Howson and Jemah [2] presented the exact solution of out-of-plane natural frequencies of plannar structures made up of curved Timoshenko beams. Wu and Chiang [3] applied finite elements to study the natural frequencies of a horizontally circularly curved Timoshenko beam. Wu and Chen [4] determined the exact solution out-of-plane free vibration response of the curved beams. Doğruer [5] presented the exact solution of the dynamic response of an out-of-plane curved beam. Tüfekci and Doğruer [6] examined the out-of-plane free vibration of a circular arch by considering the effects of transverse shear and rotatory inertia due to both flexural and torsional vibrations. Eroğlu [7] studied the static and free vibration problems of curved rods with a finite element approximate and cross-section. Dynamic response of a straight beam was examined in the Laplace domain by Manolis and Beskos [8] and Beskos and Narayanan [9]. Aslan et al. [10] investigated the undamped forced vibration of out-of-plane loaded stepped circular rods in the Laplace domain with the CFM.

This paper is as special case of Noori [11].The present article investigates the out-of-plane free vibration response of the circular rods with multiple steps. The main objective of this study is to purpose an accurate scheme to obtain the out-of-plane natural frequencies of multi stepped curved beams. Complementary Functions Method was performed Yarımpabuç et al. [12] to solve the umerical model of FG pressure vessel for stresses and displacement.

The governing equations of the free vibration response of the considered structures are obtained in the time domain. Laplace transform, with respect to time, is then applied and the obtained canonical form of the first order ordinary differential equations (ODEs) has been solved by the CFM in the transformed domain. Computer programs are prepared with FORTRAN programming language to obtain the free vibration response. The natural frequencies obtained by proposed procedure are compared with the results of ANSYS [13]. Comparisons of the results demonstrated the accuracy and exactness of the present study.

*Corresponding authour
Email: a.reshadnoori@yahoo.com.tr

European Mechanical Science, December 2018; 2(4): 111-114
doi: https://doi.org/10.26701/ems.443693
Received: July 13, 2018
Accepted: September 6, 2018

MATERIALS AND METHODS

The governing equations of the out-of-plane dynamic response of multi-stepped curved beam are obtained and given below.

$$\frac{\partial U_b}{\partial \phi} = r_0 \Omega_n + r_0 \frac{T_b \alpha_b}{GA(\phi)} \tag{1}$$

$$\frac{\partial \Omega}{\partial \phi} = \Omega_n + r_0 \frac{M_t}{GI_t(\phi)} \tag{2}$$

$$\frac{\partial \Omega_n}{\partial \phi} = -\Omega_t + r_0 \frac{M_n}{EI_n(\phi)} \tag{3}$$

$$\frac{\partial T_b}{\partial \phi} = r_0 \rho A(\phi) \frac{\partial^2 U_b}{\partial t^2} - r_0 q_b \tag{4}$$

$$\frac{\partial M_n}{\partial \phi} = r_0 \rho I_t(\phi) \frac{\partial^2 U_n}{\partial t^2} + M_n - r_0 m_t \tag{5}$$

$$\frac{\partial M_n}{\partial \phi} = r_0 \rho I_n(\phi) \frac{\partial^2 \Omega_b}{\partial t^2} - M_n + r_0 T_b - r_0 m_n \tag{6}$$

Where T_b is vertical internal forces, M_t and M_n are the components of the torsional and internal bending moments U_b is the vertical displacement, Ω_t and Ω_n are the components related rotations, E, ρ, $h(\phi)$,$A(\phi)$, $I_t(\phi)$, $I_n(\phi)$, α_b , r_0, q_b, m_t and m_n indicate the modulus of elasticity, mass density, radius of the cross-section, area of cross-section sectional area, torsional moment of inertia, bending moment of inertia, shear correction factor, radius of curvature, distributed vertical load, distributed moment of torsion and bending, respectively.

The unknown column matrix, $\{\mathbf{Y}(\phi,t)\}$, for the forced vibration out-of-plane loaded rods is given as:

$$\{\mathbf{Y}(\phi,t)\} = \{U_b, \Omega_t, \Omega_n, T_b, M_t, M_n\}^T \tag{7}$$

Applying the Laplace transform to equations (1-6), converts these partial differential equations to variable-coefficient ODEs (8-13);

$$\frac{d\bar{U}_b}{d\phi} = -r_0 \bar{\Omega}_n + r_0 \frac{\bar{T}_b \alpha_b}{GA(\phi)} \tag{8}$$

$$\frac{d\bar{\Omega}_t}{d\phi} = \bar{\Omega}_n + r_0 \frac{\bar{M}_t}{GI_t(\phi)} \tag{9}$$

$$\frac{d\bar{\Omega}_n}{d\phi} = -\bar{\Omega}_t + r_0 \frac{\bar{M}_n}{EI_n(\phi)} \tag{10}$$

$$\frac{d\bar{T}_b}{d\phi} = r_0 s^2 \rho A(\phi) \bar{U}_b - r_0 \bar{q}_b \tag{11}$$

$$\frac{d\bar{M}_t}{d\phi} = r_0 s^2 \rho A(\phi) \bar{\Omega}_t + \bar{M}_n - r_0 \bar{m}_t \tag{12}$$

$$\frac{d\bar{M}_n}{d\phi} = r_0 s^2 \rho I_n(\phi) \bar{\Omega}_n - \bar{M}_t + r_0 \bar{T}_b - r_0 \bar{m}_n \tag{13}$$

Where the terms shown by $\bar{(\cdot)}$ indicate the Laplace transform of the quantities.

The matrix notation of the ordinary differential equations ODEs (8-13) obtained in the Laplace domain is given as:

$$\frac{d\{\bar{\mathbf{Y}}(\phi,s)\}}{d\phi} = [\bar{\mathbf{A}}(\phi,s)]\{\bar{\mathbf{Y}}(\phi,s)\} + \{\bar{\mathbf{F}}(\phi,s)\} \tag{14}$$

Here, ϕ is independent variable and s is the Laplace transform parameter.

The general solution of the differential equation (14) which governs the out-of-plane free vibration response of the beam is given as follows:

$$\{\bar{\mathbf{Y}}(\phi,s)\} = \sum_{m=1}^{6} C_m [\bar{\mathbf{U}}^{(m)}(\phi,s)] + \{\bar{\mathbf{V}}(\phi,s)\} \tag{15}$$

In order to examine the free vibration of the considered structures the load vector are assumed to be zero and the Laplace parameter "s" is replaced with "$i\omega$". Also the inhomogeneous solution $\{\bar{\mathbf{V}}(\phi,s)\}$ is equal to zero. To determine the integration constants "C_m" of homogeneous solution from the boundary conditions, simultaneous equations are obtained and the matrix of the coefficients of those equations are performed. Since the mass and stiffness matrix of the system are not obtained separately by the presented procedure the eigenvalues and eigenvectors of the problem are not calculated thus the values of ω which make the determinant of coefficient's matrix zero are the natural frequencies of the structure.

NUMERICAL EXAMPLES AND DISCUSSION

In this paper the vibration of two, three and four stepped beams with circular and rectangular cross-sections is carried out. The results of three stepped circular beam with rectangular cross-sections are compared with those of ANSYS. The natural frequencies of fix-ended isotropic stepped circular beam, shown in Figure 1, are carried out. material properties are: mass density, ρ=7850x10^{-6} kgf/cm^3, Poisson's ratio, ν = 0.3, and modulus of elasticity, E=2.1x10^6 kgf/cm^2.

The radius of cross section ($h(\phi)$) of the two, three and four stepped beam is considered to be:

$$h(\phi) = \begin{cases} 0.5, & -\frac{\pi}{6} \le \phi \le \frac{\pi}{6} \\ 1.0, & \frac{\pi}{6} \le \phi \le \frac{\pi}{4} \\ 1.0, & -\frac{\pi}{4} \le \phi \le -\frac{\pi}{6} \end{cases};$$

$$h(\phi) = \begin{cases} 0.5, & -\frac{\pi}{12} \le \phi \le \frac{\pi}{12} \\ 1.0, & \frac{\pi}{12} \le \phi \le \frac{\pi}{6} \\ 1.0, & -\frac{\pi}{12} \le \phi \le -\frac{\pi}{6} \\ 2.0, & \frac{\pi}{12} \le \phi \le \frac{\pi}{4} \\ 2.0, & -\frac{\pi}{12} \le \phi \le \frac{\pi}{4} \end{cases};$$

doi: https://doi.org/10.26701/ems.443693

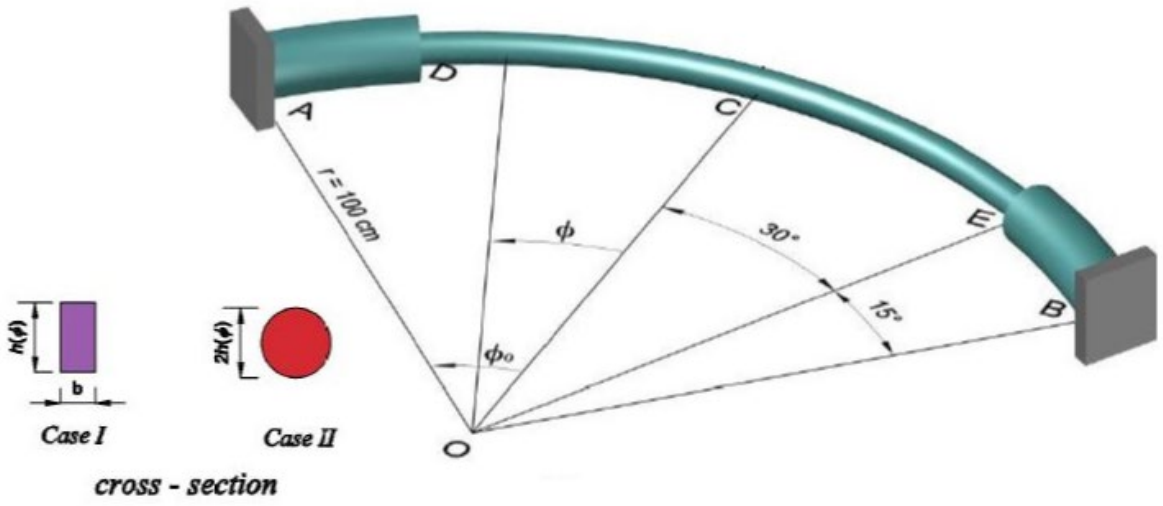

Figure 1: Fix–ended circular stepped rod

$$h(\phi)=\begin{cases}0.5, & -\frac{\pi}{16}\le\phi\le\frac{\pi}{16}\\ 1.0, & \frac{\pi}{16}\le\phi\le\frac{\pi}{8}\\ 1.0, & -\frac{\pi}{16}\le\phi\le-\frac{\pi}{8}\\ 2.0, & \frac{\pi}{8}\le\phi\le\frac{3\pi}{16}\\ 2.0, & -\frac{\pi}{8}\le\phi\le-\frac{3\pi}{16}\\ 4.0, & \frac{3\pi}{16}\le\phi\le\frac{\pi}{4}\\ 4.0, & -\frac{3\pi}{16}\le\phi\le-\frac{\pi}{4}\end{cases}$$

The flexural rigidity and cross section of rectangular and circular rod are given respectively, as;

$$GI_t(\phi)=G*0.141,\quad EI_n(\phi)=E\frac{bh^3(\phi)}{12},\quad A(\phi)=bh(\phi);$$

$$GI_t(\phi)=G*\frac{\pi h^4(\phi)}{2},\quad EI_n(\phi)=E\frac{\pi h^4(\phi)}{4},\quad A(\phi)=\pi h^2(\phi)$$

The geometric properties of the rods are tabulated in Table 1.

Table 1: Geometric properties of the rod.

Cross-section	$b(0)$ (cm)	$h(0)$ (cm)	r_0 (cm)	ϕ_0	α_n
Rectangular (Case I)	1	1	100	45	1.2
Circular (Case II)	-	0.5	100	45	1.11

At first the natural frequencies of a fix-ended, three steps beams with circular and rectangular cross-sections are carried out by the proposed approach. Obtained results compared with those of ANSYS. Comparison of the natural frequencies of the considered structure are listed in Table 2 for multiple stepped.

To demonstrate the accuracy of the proposed method, the natural frequencies obtained are compared with those of ANSYS. The parametric study on the free vibration of the stepped curved rods with circular and rectangular cross-section are studied and presented in Table 3.

As expected, the number of steps have a remarkable influence on the out-of-plane natural frequencies of the structures. As it can been seen in Table 3, the two-stepped beam with rectangular cross section has the lowest natural frequencies which corresponds to the highest period. Similarly the mentioned table shows that four-stepped beam with circular cross section has the highest natural frequencies and the lowest oscillating periods.

CONCLUSION

In this study, an efficient unified approach based on the combination of Laplace transform and the CFM is employed to examine out-of-plane free vibration response of the circular multi- stepped beams. The RK5 algorithm has been employed in the numerical solution process of initial value problems based on the CFM. Materials of the beam are considered to be isotropic, homogeneous and elastic.

Table 2: The natural frequencies of fix-ended rod with three stepped cross-section (Hz).

Mode	Present Study (Case I)	ANSYS (100 Elements)	Present Study (Case II)	ANSYS (100 Elements)
1	1.119	1.115	2.821	2.836
2	3.849	3.828	7.051	7.610
3	7.866	7.872	13.654	13.673
4	15.901	15.803	27.240	27.148
5	24.443	24.311	41.821	41.725

doi: https://doi.org/10.26701/ems.443693

Table 3: The natural frequencies of fix-ended rod with two stepped cross-section (Hz).

Mode	Two-stepped Beam		Three-stepped Beam		Four-stepped Beam	
	Case I	Case II	Case I	Case II	Case I	Case II
1	0.5771	1.0149	1.119	2.821	1.529	4.912
2	2.4498	4.6642	3.849	7.051	5.349	11.630
3	5.3832	8.9398	7.866	13.654	10.993	20.171
4	10.497	17.9403	15.901	27.240	21.247	40.246
5	16.494	30.1026	24.443	41.821	30.805	51.372

The canonical form of the first ODEs governing equations of the motion of the stepped circular beam has been solved by the CFM in the Laplace domain for a set of Laplace parameters. Several parametric results are presented. The proposed method can be apply to obtain the free vibration response of arbitrary stepped beams.

For the considered structures, computer program is coded in FORTRAN. The accuracy and exactness of the proposed procedure are demonstrated by comparing its results with the results of ANSYS. Good agreement is observed.

REFERENCES

[1] Kawakami M, Sakiyama T, Matsuda H, Morita C, (1995). In-Plane and out-of-plane free vibrations of curved beams with variable cross-sections. Journal of Sound and Vibration 187: 381-401.

[2] Howson W P, Jemah A K, (1999). Exact out-of-plane natural frequencies of curved Timoshenko beams. Journal of Engineering Mechanics 125: 19-25.

[3] Wu J S, Chiang L K, (2004). A new approach for free vibration analysis of arches with effects of shear deformation and rotary inertia considered. Journal of Sound and Vibration 277: 49-71.

[4] Wu J S, Chen Y C, (2011). Out-of-plane free vibration analysis of a horizontally circular curved beam carrying arbitrary sets of concentrated elements. Journal of Structural Engineering, 10.1061, ASCE_ST.1943- 541X.0000290.

[5] Doğruer O Y, (2006). Analytical solutions of out- of-plane static and dynamic problems of planar curved beams, Istanbul Technical University, Istanbul, PhD. Thesis.

[6] Tüfekci E, Doğruer O Y, (2006). Out of plane free vibration of a circular arch with uniform cross-section: Exact solution, J. Sound Vib. 291: 525-538.

[7] Eroğlu U, (2014). Finite element analysis of curved beams using exact solutions, Istanbul Technical University, Istanbul, MSc. Thesis.

[8] Manolis G D, Beskos D E, (1982). Dynamic response of framed underground structures, Comp. and Struct. 15(5): 521-531.

[9] Beskos D E, Narayanan G V, (1983). Dynamic response of frameworks by numerical Laplace transform. Computer Methods in Applied Mechanical and Engineering, 37(3): 289-307.

[10] Aslan T A, Noori A R, Temel B, (2017). Forced vibration of out of plane loaded stepped circular rods. International Conference on Civil and Environmental Engineering, May 8-10, Nevsehir, Turkey, 2062- 2074.

[11] Noori A R, Aslan T A, Temel B, (2018). Damped transient response of in-plane and out-of-plane loaded stepped curved rods. Journal of the Brazilian Society of Mechanical Sciences and Engineering 40: 1-24.

[12] Yarımpabuç D, Eker M, Çelebi K, (2018). Mechanical behavior of functionally graded pressure vessels under the effect of Moisson's ratio. European Mechanical Science 2(2): 52-59.

[13] ANSYS Swanson Analysis System, Inc., 201 Johnson Road, Houston, PA15342-1300,USA.

EUROPEAN MECHANICAL SCIENCE
e-ISSN: 2587-1110

Research Paper

Investigation of the Effect on Tribological Properties of the use of Pinus Brutia Cone as a Binder in Brake Pads

İlker Sugözü*, Kürşat Kahya

Mersin University, Faculty of Engineering, Mechanical Engineering Department, Mersin, Turkey
ORCID: İ.Sugözü (0000-0001-8340-8121)

Abstract

Phenolic resin is invariably used as binder material for friction composites. Alternative materials are considered alternatively to phenolic resin due to negativities such as poor shelf life, harmful volatiles during processing, the need for addition of curing agent before shipment, shrinkage and voids in final products. For these reasons, pinus brutia cones are ground and pulverized and added to the brake lining content at different rates and thus 3 different samples were produced. The wear and friction tests of these samples were made on pin-on disc type brake lining test machine. After this, the density of the samples was determined by using Archimedes scale. The hardness was determined in the Brinell tester. And finally, the microstructure properties of the samples were determined by using a scanning electron microscope (SEM).

Keywords: Pinus brutia cone, brake pad, friction, wear

1. INTRODUCTION

A brake pad is a composite of many different ingredients. Components are classified as fibers, binders, solid lubricants, fillers, abrasives, metallic fillers and friction modifiers. In generally phenolics or their modified versions are used as binder materials for friction composites.

In order for a brake lining to provide safe driving under harsh environment and driving conditions, many features such as regular friction coefficient, low wear rate, thermal deformation resistance and low noise and vibration as comfort conditions are required. Materials such as resin, fiber (fiber), solid lubricant, abrasive particles, metal shavings and fillers are used to provide these desired properties [1].

Storage of various products obtained as waste or leaving them directly to the nature has great negative effects on the society including environmental pollution. Nowadays, scientific studies are carried out for the non-asbestos brake lining [2-8]. There are many studies in the literature to evaluate agricultural wastes. Idris et al. developed a non-asbestos free brake pads using banana peels and results show that banana peels can be used [9]. Koya and Fono produced automotive brake pad using palm kernel shell and the result obtained showed that the palm kernel shell can be used in brake pad [10]. Ruzaidi et al. produced brake pads using palm slag and results showed that palm slag can be used in brake pad composites [11]. Pinus brutia cones are also among the waste products and it is considered as binder due to its resinous structure.

In this study, usage of pinus brutia cone powder as a binder material in brake pad was investigated experimentally.

2. MATERIALS AND METHODS

The friction materials investigated in this work were variations of a NAO (non-asbestos organic) type material containing different ingredients including pinus brutia cone powder. Pinus brutia was obtained from Tarsus/Mersin in Turkey. Three different samples were produced. These samples contained pinus brutia cone powder, phenolic resin, steel fibers, Al_2O_3, Cu particles, graphite, brass particles, cashew and barite. The friction coefficient and temperature values were stored in a databank. The brake lining samples were produced in the conventional procedure for a dry formulation following dry mixing, pre-forming and hot pressing. Detailed conditions for each manufacturing step can be found in the author's other study [12]. The compositions of the friction materials studied in this work are shown in Table 1.

Figure 1 shows a schematic view of the brake tester used in this study. Detailed conditions for each brake test step can be found in the author's other study [12]. The temperature

*Corresponding authour
Email: isugozu@mersin.edu.tr

European Mechanical Science, December 2018; 2(4): 115-118
doi: https://doi.org/10.26701/ems.471131
Received: October 16, 2018
Accepted: November 16, 2018

and friction-coefficient values were stored in the databank. The tests were repeated three times for each sample. Friction coefficient - temperature - time graphs were obtained to identify the effects of these variables.

Table 1. Ingredients of the samples (weight %)

	KI-0	KI-8	KI-12
Cu particles	8	8	8
Steel fibers	15	15	15
Al_2O_3	5	5	5
Brass particles	5	5	5
Graphite	7	7	7
Barite	30	30	30
Cashew	10	10	10
Pinus brutia cone powder	0	8	12
Phenolic resin	20	12	8

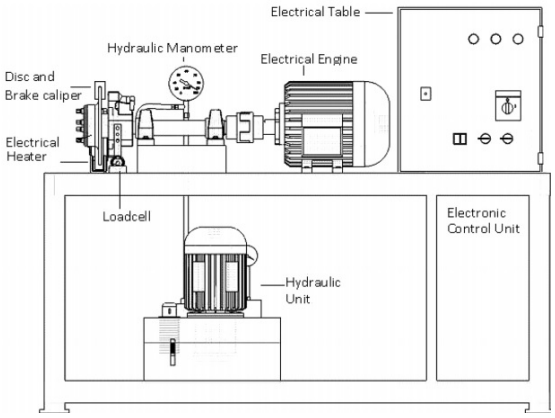

Figure 1. Schematic view of the brake tester

The friction coefficient was calculated by measuring the normal and tangential pressures throughout the test 500 s. It was expressed as the mean value of the entire braking dependence during the friction-coefficient test. The specific wear rate was determined with the mass method following the Turkish Standard [13] and British Standard [14] and calculated with the following Equation (1):

$$V = \frac{1}{2.\pi.R} \cdot \frac{m_1 - m_2}{n.f_s.\rho} \quad (1)$$

where V is the specific wear ratio (cm^3/Nm), R is the distance between the centre of specimen and the centre of the rotating disk (m), n is the rev of the rotating disk (rev/min), m_1 and m_2 are the average weights of specimen before and after the test (g), ρ is the density of the brake lining (g/cm^3), and f_m is the average friction force (N) [12-16].

3. RESULTS AND DISCUSSION

3.1 Effect of the temperature on the friction performance

Based on experimental study results for friction coefficients and temperature graphs are shown in Figures 2-4. Figures 2-4 show time-dependent friction coefficient-temperature graphs of brake pad samples using phenolic resin and pinus brutia cone powder as binder material. The highest coefficient of friction is 0.31 with code KI-8 It is seen in the sample.

Figures 2-4 show temperature changes due to the effect of friction on time. When the shapes were examined, the highest temperature was found at KI-0 and the highest coefficient of friction at KI-8 coded sample.

The friction characteristics after the development of the friction layer were characterized by the characteristics of the constituents of the friction layer in all the samples of the pinus brutia cone powder added. When these graphs showing the variation of the friction coefficient were examined, the KI-0 coded sample showed less fluctuation than the KI-8 and KI-12 coded samples. The increase in the coefficient of friction of the KI-8 and KI-12 coded samples was accompanied by an increase in the internal temperature. This rise in the coefficient of friction can be explained as the ability of the materials constituting the friction layer to improve on the temperature of the disk, which forms the opposing surface of the friction couple, i.e. to create a resistance against the friction surface as the constituent materials are well compatible with each other.

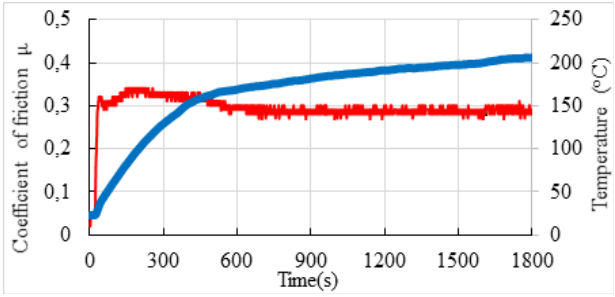

Figure 2. Change in the friction coefficient and the temperature as a function of time for sample KA-0

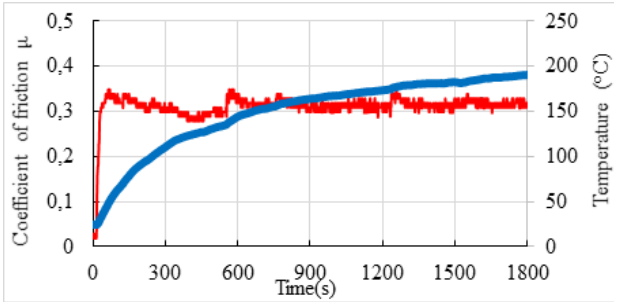

Figure 3. Change in the friction coefficient and the temperature as a function of time for sample KA-8

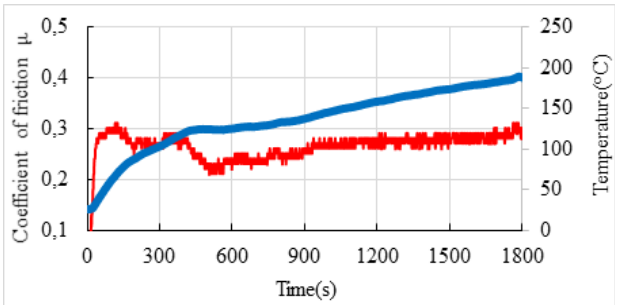

Figure 4. Change in the friction coefficient and the temperature as a function of time for sample KA-12

KI-0 coded specimen decreased in friction coefficient up to 600 seconds. After 600 seconds, the friction coefficient became stable with increasing temperature. The KI-0 coded sample exhibited a low but stable friction with temperature increase.

The KI-8 coded sample has gradually increased in the coefficient of friction from the moment it has started to rise above 130 °C after 400 seconds. The same is true after 500 seconds on the code KI-12. It is thought here that the warmth of the brake pad samples added pinus brutia cone powder causes the development of curing and binder properties. When the graph of KI-0 coded sample was examined, a decrease in coefficient of friction was observed depending on the temperature. When the graphs shown in Figure 3 and Figure 4 are examined, there is an increase in the coefficient of friction depending on the temperature. It is generally emphasized in the literature that the coefficient of friction (μ) varies between 0.1 and 0.7 depending on the frictional force and the disk lining interface temperature [13, 14]. Compared to Figure 2 and Figure 3, the pinus brutia cone powder shows a slight increase in the coefficient of friction of the sample powder sample. Compared to Figures 2 and 4, the frictional performance of the red-brown cone-coated brake pad sample decreases. Comparing the shapes, it is seen that a graph which shows a rise in the coefficient of friction of the pinus brutia powder doped samples as the temperature increases. When the variation coefficient of friction of all samples was examined, the friction in the first 50 seconds showed similar characteristics in surface layer formation as mentioned above. KI-0 coded sample has a partial decrease in temperature from 50th to 500th with an increase in temperature, followed by recuperation. However, a slight increase in the coefficient of friction was observed with increasing temperature after 400 seconds in the sample KI-8 and 500 seconds in the sample the KI-12 code. As shown in Figure 3 and Figure 4, the lowest coefficient of friction is the KI-8 code sample, while the highest coefficient of friction is the KI-12 code.

3.2 Microstructural characterization of friction surfaces

Figure 5 shows the SEM photographs taken to determine the characteristics of the friction surface formed after experiments in which the tribological properties of the pinus brutia cone powder additive brake pads are determined. When looking at photographs in general, it appears that the photographs of the friction surfaces show traces of scratches that show abrasive wear with microfissures, micro-cavities and coated friction layers showing adherent wear. It is also understood that the component-forming materials on the friction surfaces formed actively participate in the friction. 20% by mass of the phenolic resin binder content that KI-0 the SEM photo of the coded sample is shown in Figure 5 (a). This sample exhibited a friction coefficient average of 0.29. The micro voids formed by the particles that are cut from the sample are seen in the picture. Short scratches and color differences on the friction surface indicate that adhesion and abrasive wear have occurred.

In the content of KI-8 coded sample, 12% by mass of phenolic resin and 8% of cornelian cones were observed as a binder, and homogeneous distribution of constituent materials in SEM photograph (Figure 5-b). And the sample exhibited a friction coefficient average of 0.31. Shaped short-sized friction surfaces show abrasive wear. The small clumps that are seen are the result of the barite in the contents. The boundaries of the assembled materials are seen. On the surface of these particles, which are seen as dark and light gray color, it is thought that the materials which are put on these particles after the comeback from other friction regions cause adhesion wear. The white bright colored regions are metal particles that are actively incorporated into the friction.

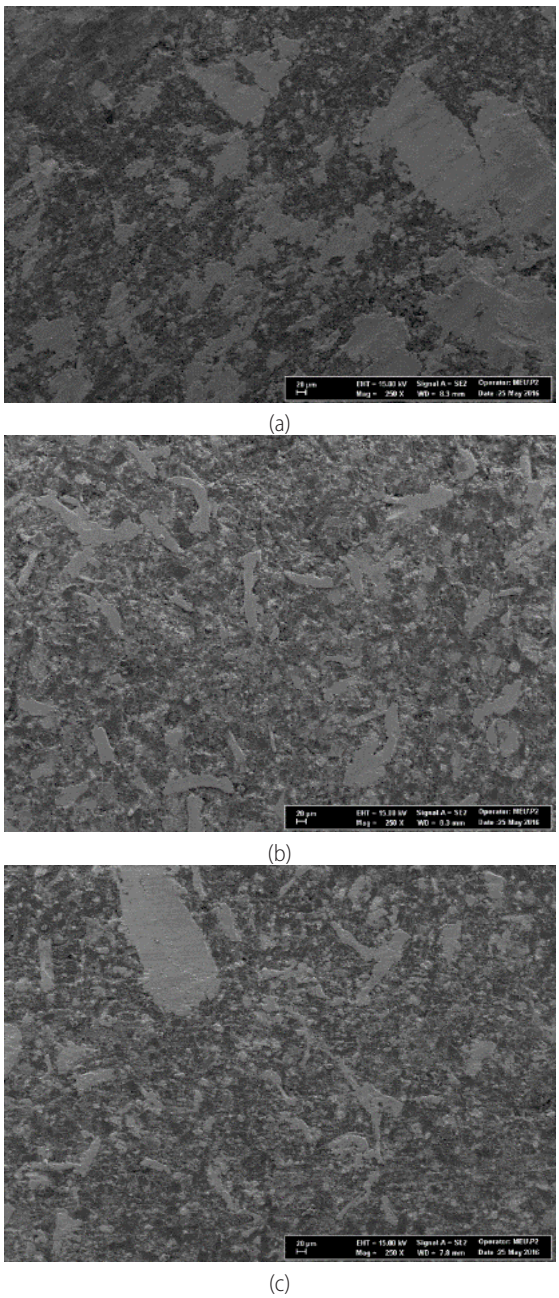

(a) (b) (c)

Figure 5. SEM micrographs of brake-pad samples (a) KI-0 (b) KI-8 (c) KI-12

Containing 8% phenolic resin and 12% pinus brutia cone powder as binder in order to determine the characteristic of the friction surface of the KI-12 code sample. The SEM photograph taken is shown in Figure 5 (c). In general, it is seen that there are micro-cracks due to thermomechanical stresses and friction coatings formed on the friction surfaces due to short scratches, abrasive wears, micro and macro voids and adherent abrasion resulting from abrasive wear. It is also

understood that the component-forming materials on the friction surfaces formed actively participate in the friction. The KI-12 coded sample exhibited a coefficient of friction coefficient of 0,26. Component-forming materials may have a hard structure, which may result in high hardness values. However, If the binder of resin holding component-forming materials and general the content orientation is not appropriate, rapid detachment of the component forming particles from the main structure during small stresses during friction can result in high wear rates as expected.

3.3 Wear behaviour

The hardness, density and wear values of the samples are shown in Table 2. When the tables were examined, the coefficient of friction of KI coded samples was 0,28 and the average wear amount was 0,86. In the samples, if the hardness of the brake pad is high, the wear resistance must be high and it can be done as a result. However, If the binder of resin holding component-forming materials and general the content orientation is not appropriate, rapid detachment of the component forming particles from the main structure during small stresses during friction can result in high wear rates as expected.

Table 2. Typical characteristics of the brake pads used in this study

Sample code	Mean coefficient of friction	Density (g/cm^3)	Brinell Hardness (HB)	**Specific wear rate (cm^3/Nm)** x10^{-6}
KI-0	0,29	2,225	28	1,691
KI-8	0,31	2,300	29	1,997
KI-12	0,26	2,356	26	1,902

4. CONCLUSIONS

In this study, the use of pinus brutia cone powder as a binder in automotive brake pads has been experimentally investigated.

The highest average coefficient of friction value for all specimens undergo friction test is 0.31, belonging to the KI-8-coded specimen containing 8% pinus brutia cone powder, the lowest average friction coefficient is 0.26, belonging to the KI-12 coded specimen containing 12% pinus brutia cone powder. The specific wear rate and density increased with inreasing pinus brutia cone powder for all samples. The experimental results have shown that the friction layer, with the use of pinus brutia cone powder significantly improved the overall performance. With the increasing of temperature, the ingredients in the braking pad were affected other due to faster diffusion. As a result, pinus brutia cone powder can be used as binder for brake pads.

ACKNOWLEDGEMENTS

This study was supported by the Research Fund of Mersin University in Turkey with Project Number 2016-2-AP4-1945

REFERENCES

[1] Y. C. Kim, M. H. Cho, S. J. Kim, H. Jang, The effect of phenolic resin, potassium titanate, and CNSL on the tribological properties of brake friction materials, Wear, Volume 264, Issues 3–4, 2008.

[2] K. K. Ikpambese, D. T. Gundu, L. T. Tuleun, Evaluation of palm kernel fibers (PKFs) for production of asbestos-free automotive brake pads, Journal of King Saud University-Engineering Sciences, 28 (1), 110-118, 2016.

[3] Y. Handa, T. Kato, Effect of Cu powder, BaSO4 and cashew dust on the wear and friction characteristics of automotive brake pads, Tribol. Trans. 39 (2), 346–353, 1996.

[4] B. Sugözü, B. Dağhan, Effect of BaSO4 on tribological properties of brake friction materials. IJIRSET, 5(12), 30-35, 2016

[5] İ. Uluocak, H. Yavuz, M. Gürsul, Effects of Rotor Material on Eddy Current Brake Performance, European Mechanical Science, 1 (4), 129-132, 2017.

[6] B. Sugozu, Investigation of ulexite usage in automotive brake friction materials. Turkish Journal of Engineering, 2(3), 125-129, 2018.

[7] H. Jang, S.J. Kim, The effects of antimony trisulfide (Sb2S3) and zirconium silicate (ZrSiO4) in the automotive brake friction material on friction characteristics, Wear, 239 (2), 229–236, 2000.

[8] B. Sugözü, B. Dağhan, A. Akdemir, Effect of the size on the friction characteristics of brake friction materials: a case study with Al2O3. Industrial Lubrication and Tribology, 70(6), 1020-1024, 2018.

[9] U.D. Idris, V. S. Aigbodion, I. J. Abubakar, C. I. Nwoye, (2015), Ecofriendly asbestos free brake-pad: using banana peels. J. King Saud Univ.-Eng. Sci. 27 (2), 185–192.

[10] O. A. Koya and T. R. Fono, (2010), Palm kernel shell in the manufacture of automotive brake pad (accessed at www.rmrdctechnoexpo.com, 7/3/210).

[11] C. M. Ruzaidi, J. B. Kamarudin, J. B. Shamsul, A. M. Mustafa Al Barkri, A. R. Rafiza, Comparative study on thermal, compressive, and wear properties of palm slag brake pad composite with other fillers. Aust. J. Basic Appl. Sci. 5, 79, 2011.

[12] I. Sugozu, I. Mutlu, K. B. Sugozu, The effect of ulexite to the tribological properties of brake lining materials. Polymer Composites, 39(1), 55-62, 2018.

[13] TS 555 (Turkish Standard), Highway vehicles, brake systems, brake pads for frictional brake, Turkey, 1992

[14] British Standards Specification: BS AU 142–1968, 1968

[15] K. H. Cho, H. Jang, Y. S. Hong, S. J. Kim, R. H. Basch, J. W. Fash, The size effect of zircon particles on the friction characteristics of brake lining materials, 264 (3-4), 291-297, 2008.

[16] B. Sugozu, B. Daghan, A. Akdemir, N. Ataberk, Friction and wear properties of friction materials containing nano/micro-sized SiO2 particles. Industrial Lubrication and Tribology, 68(2), 259-266, 2016.

EUROPEAN MECHANICAL SCIENCE
e-ISSN: 2587-1110

Research Paper

Crack Analysis in the Sae 1117 Steel Shafts for Inclusion and Heat Treatment Combination Effect

Tuğrul Soyusinmez[1*], Murat Ardan Kayaaltı[2], Oğuzcan Güzelipek[3], Gökçe Akkuş[4], Taner Kavas[5]

[1,2,3,4]Totomak Machinery and Spare Parts Co., Turkey
[5]Afyon Kocatepe University; tkavas@aku.edu.tr
ORCID: T.Soyusinmez (0000-0001-8333-1961)

Abstract

Surface hardening in steels is a process in which a chemical composition is changed by thermo-chemical processes in a determined region and, accordingly, some micro-structure is changed. In order to obtain a harder layer than the inner region starting from the surface to a certain depth, it is mostly provided by diffusion of elements such as nitrogen and carbon. The process is particularly important in low and medium carbon steels in terms of increasing wear resistance, tensile strength and fatigue strength. The amount of elements used in cementation together with the duration of cementation is extremely important in terms of the harmonious change of structural differentiation. The effect of size and position of inclusions on the cracked structures which is affected from heat treatment is presented in the paper.

Keywords: Inclusion, Cracks, SAE 1117, Heat Treatment

1. INTRODUCTION

The surface hardening processes in the steels are the processes in which the chemical composition and thus some microstructure are changed by thermochemical processes in a determined region. In order to obtain a harder layer from the interior to a certain depth starting from the surface, it is mostly provided by the diffusion of elements such as nitrogen and carbon. The process is particularly important for low and medium carbon steels to improve wear resistance, tensile strength and fatigue strength. In addition, the amount of the element used in cementation and the time of cementation are extremely important for the change of structural differentiation.

On the other hand, it is also a fact that inclusions are formed due to different reasons during production / casting. The reasons for the inclusion are cast sand, pollution or slag mixing from the refractories are shown as the main reasons, but elemental (especially silica, alumina, manganese or iron oxide) impurities have been shown to cause differentiation in the melt.

We can define inclusions as foreign substances found in steels in general. These substances are generally particulate structures that are insoluble from the material matrix such as sulfur, oxide, silicate. One of the researchers, Sims, divides inclusions into two classes, which are endogenous and exogenous inclusions, respectively. The inclusion type as a result of the reactions in the molten metal is endogenous and its shapes, sizes and contents vary according to the process applied to the molten metal. Another type of inclusion, exogenous inclusions, is formed by the effect of slag formed during the production of steel. This inclusion was found to be larger, more irregular and complex in shape than endogenous inclusion [1,2]. In general, the size of the inclusions is greater than ~ 0.5 μm and is found as a chemical compound in the structure of metals and alloys. For example, the oxide (Al2O3) or sulphide (MnS) inclusions we see in the steel are the best examples. Many factors are caused by inclusion and we can list these factors as casting sand, pollution from the refractories or slag mixing. In addition to these main causes, elemental impurities also show differences in some regions. The inclusions are beneficial to the material rather than the harmful aspects. For example, oxide inclusions in the steel interact with dislocations to increase the hardness of the material and significantly change the yield strength of the material. One of the other positive factors provided by the inclusions is that they can be encountered in the automaton steels with resulfillations. Thanks to the resulphurisation, MnS inclusions in the steel are formed and the workability of the material is increased. In addition to this, increasing

*Corresponding authour
Email: tsoyusinmez@totomak.com.tr

European Mechanical Science, December 2018; 2(4): 119-127
doi: https://doi.org/10.26701/ems.477224
Received: November 6, 2018
Accepted: November 20, 2018

MnS sizes and decreasing MnS amount increase the workability [3]. As it is understood from the examples given, inclusions can be harmful or useful, and the general factors that determine this are the types, sizes, shapes, distributions and quantities. The inclusions are usually multi-phase and the composition of inclusions in the steel varies according to the elemental content of the steel. Polarized light and electron-probe micro analyzer are used to determine inclusions. In this article, inclusions occurring in steel shafts were examined with microscopic camera systems and the cracks produced by inclusions were analyzed.

2. METHODOLOGY

In this study, microstructure and inclusion studies were planned on the samples (Figure 1. a) and the samples were first cut by water jet so that the microstructure was not affected from the external conditions as shown in Figure 1. b.

Then, the samples were re-cut with the help of water jet and the surface was polished for microstructure studies. Representative samples obtained after first cutting with water jet has been shown in Figure 2. Parts are polished after being cut with water jet. Figure 3 shows the dimensioning of the samples after the second cut (a), unpolished parts (b), and photos after polishing (c). The images of this experiment, which are examined by camera system. As experimental method, two types of methods can be used for inclusions. The first of these is microscopic test methods and the polished surface is examined by a light microscope and several representative photographs are made by reporting the inclusion types encountered in the sample. Surface polishing is carried out for a satisfactory and more consistent result. The experiment is carried out with samples from three different positions of the part. In order to determine the microscopic image, the polished surface area should be minimum 160 mm^2. In addition, the section taken from the sample should be parallel to the longitudinal plane and perpendicular to the rolling plane of the section.

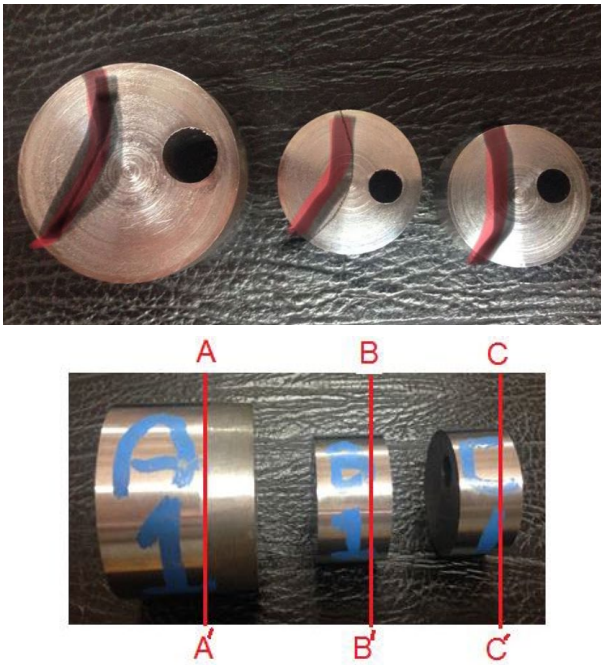

Figure 1. a) Representative examples provided by the Totomak A.Ş. b) First Water jet cutting of samples

Figure 2. a) Representative samples obtained after first cutting with water jet b) Second cutting lines of samples

Figure 3. a) Dimensioning of the samples after the second cut. b) Unpolished parts, c) Polished parts

Each sample was first examined by polarizing microscope and the images of each group are given below.

For the group A;
Figure 4 shows the image taken at 20 magnifications from sample A1. Figure 5 shows the image taken at 20 magnifications from sample A2. Figure 6 shows the image taken at 20 magnifications from sample A3.

For the group B;
Figure 7 shows the image taken at 20 magnifications from sample B1. Figure 8 shows the image taken at 20 magnifications from sample B2. Figure 9 shows the image taken at 20 magnifications from sample B3.

For the group C;
Figure 10 shows the image taken at 20 magnifications from sample C1. Figure 11 shows the image taken at 20 magnifications from sample C2. Figure 12 shows the image taken at 20 magnifications from sample C3.

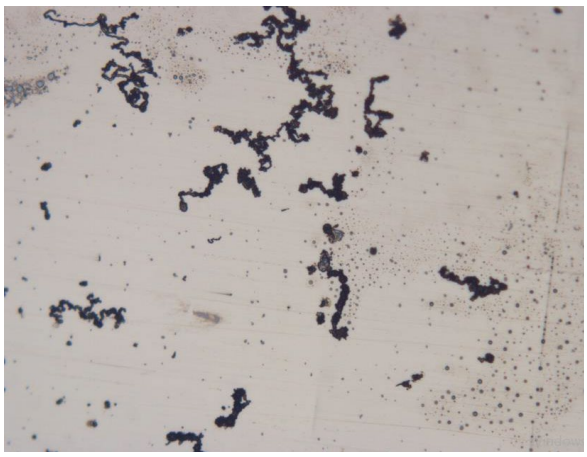

Figure 4. Sample A1 (20X)

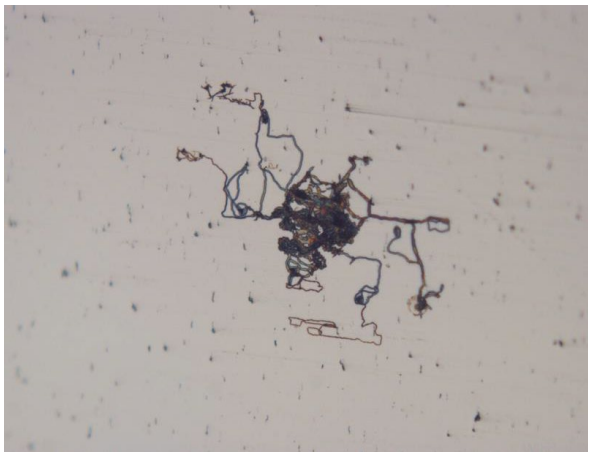

Figure 5. Sample A2 (20X)

Figure 6. Sample A3 (20X)

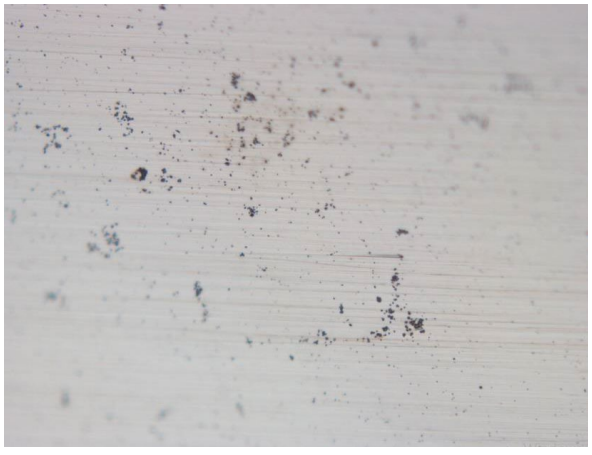

Figure 7. Sample B1 (20X)

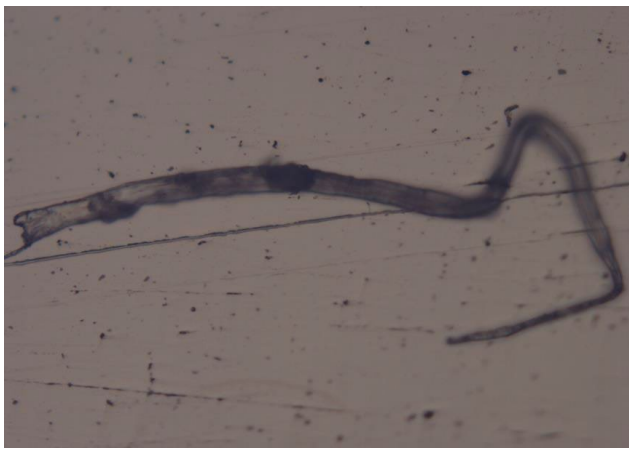

Figure 8. Sample B2 (20X)

Figure 9. Sample B3 (20X)

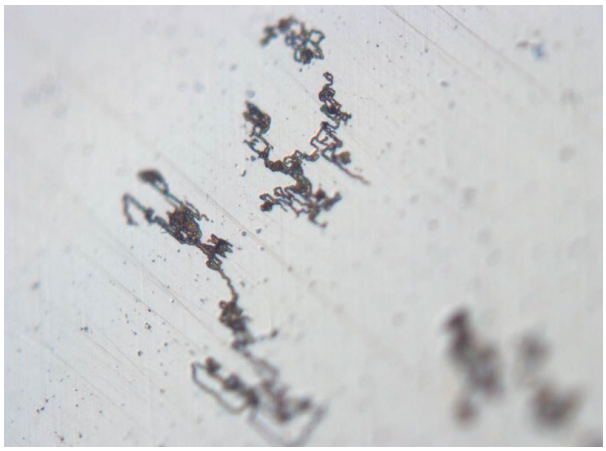

Figure 10. Sample C1 (20X)

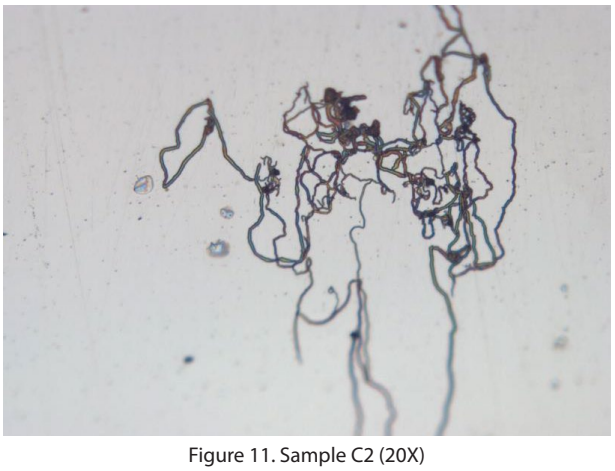

Figure 11. Sample C2 (20X)

Figure 12. Sample C3 (20X)

On the other hand, the samples with the most intense inclusion and superficial cavities under polarizing microscope were firstly taken before the polishing and then after the polishing (SEM) images and the figures obtained are given below. In addition, chemical analysis and elemental mapping analysis were performed for each group.

For the group A;

Figure 13 shows the elemental mapping of A group sample. As shown in figure 13, the red colors show the iron element, the green colors are carbon and blue colors are aluminum. The microstructure area of the elemental mapping analysis is shown in Figure 14. In addition, chemical analysis was performed on the yellow line determined in Figure 14. The results of the chemical analysis are shows in Figure 14.

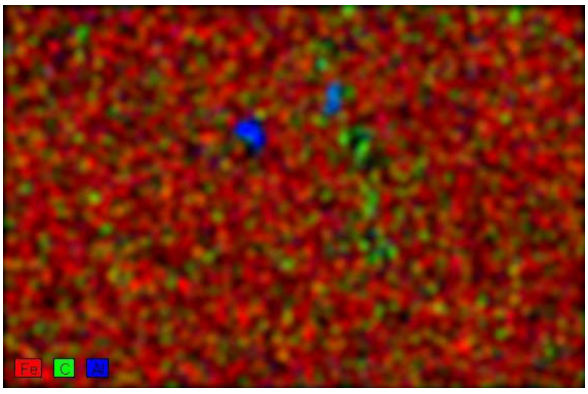

Figure 13. Elemental mapping of A coded sample

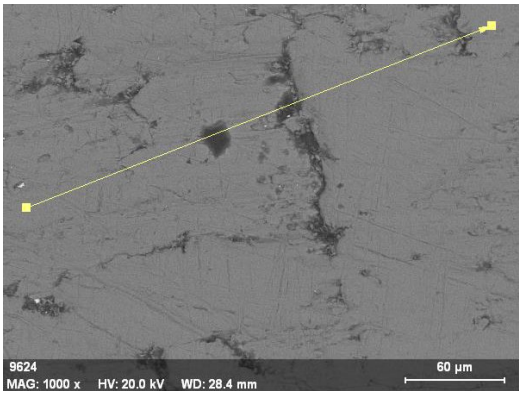

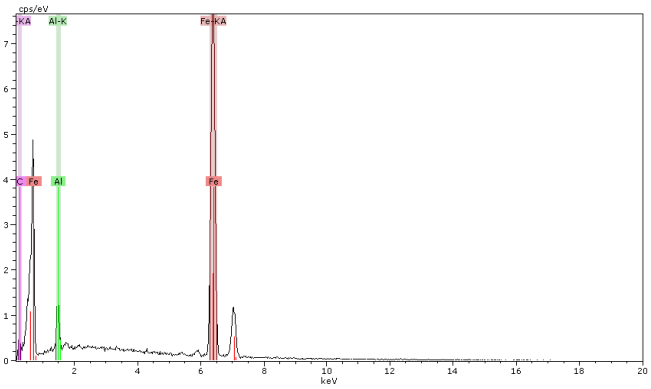

Figure 14. Chemical analysis of group A along the axis

For the group B;

Figure 15 shows the elemental mapping of B group sample. As shown in figure 15, the red colors show the iron element, the green colors are carbon and blue colors are aluminum. The microstructure area of the elemental mapping analysis is shown in Figure 16. In addition, chemical analysis was performed on the green line area in Figure 16. The results of the chemical analysis are shows in Figure 16.

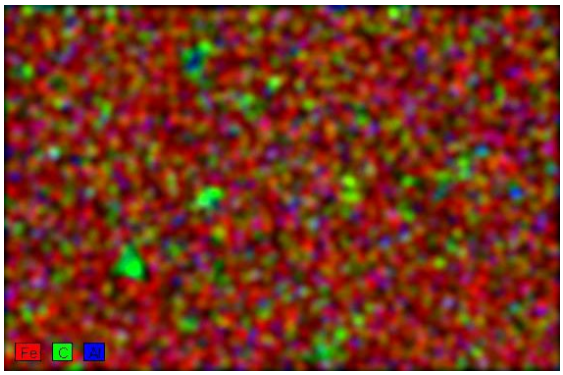

Figure 15. Elemental mapping of B coded sample

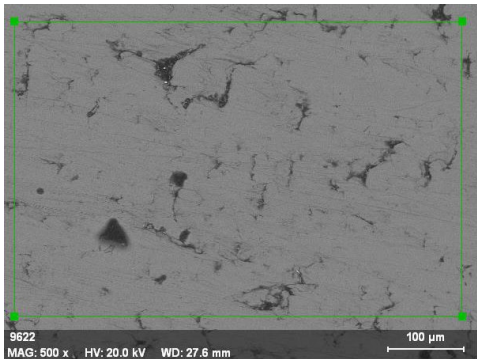

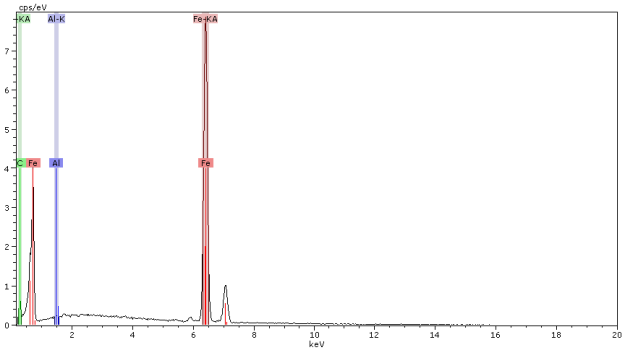

Figure 16. Chemical analysis of group B along the axis

doi: https://doi.org/10.26701/ems.477224

For the group C;

Figure 17 shows the elemental mapping of C group sample. As shown in figure 17, the red colors show the iron element, the green colors are carbon and blue colors are aluminum. The microstructure area of the elemental mapping analysis is shown in Figure 18. In addition, chemical analysis was performed on the green line area in Figure 18. The results of the chemical analysis are shows in Figure 18.

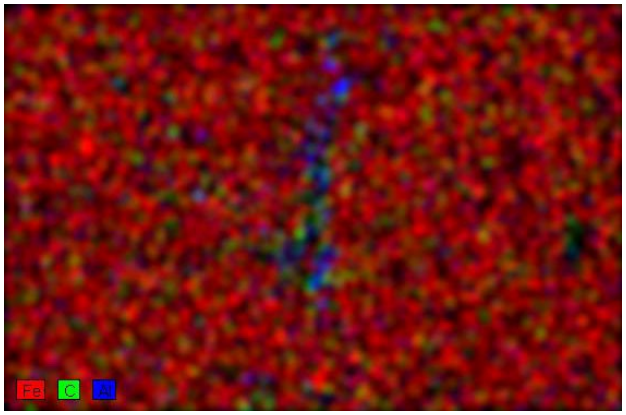

Figure 17. Elemental mapping and chemical analysis of C coded sample

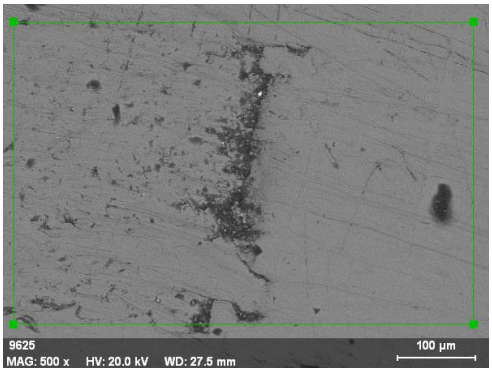

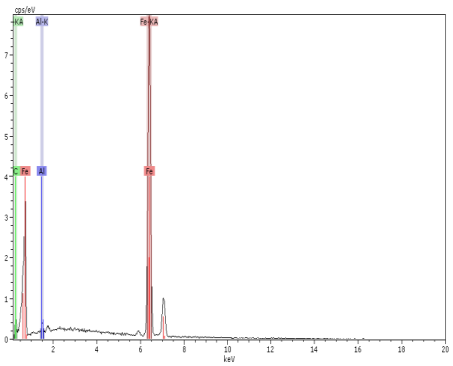

Figure 18. Chemical analysis of group C along the axis

Following the microstructure analysis above, section analyzes of each sample were carried out and the data obtained are given below.

Figure 19 show the vertical section microstructure image and chemical analysis of sample A. Figure 20 show the vertical section microstructure image and chemical analysis of sample B. Figure 21 show the vertical section microstructure image and chemical analysis of sample C.

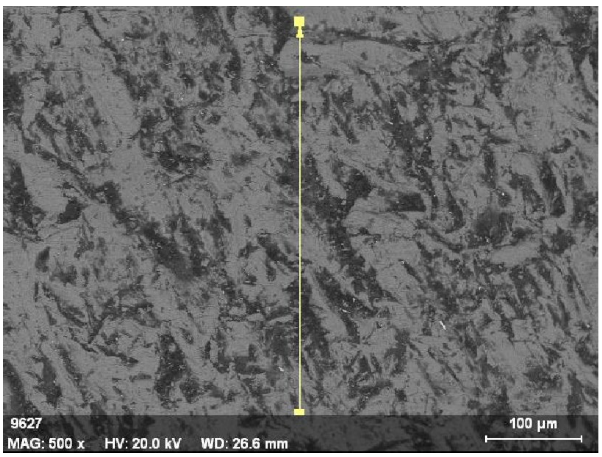

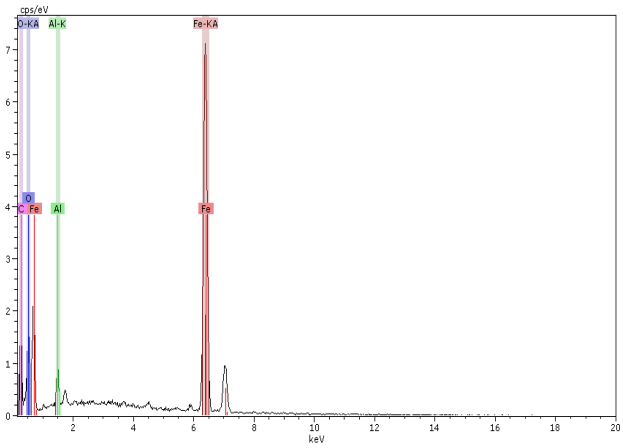

Figure 19. Vertical section microstructure image and chemical analysis of sample A

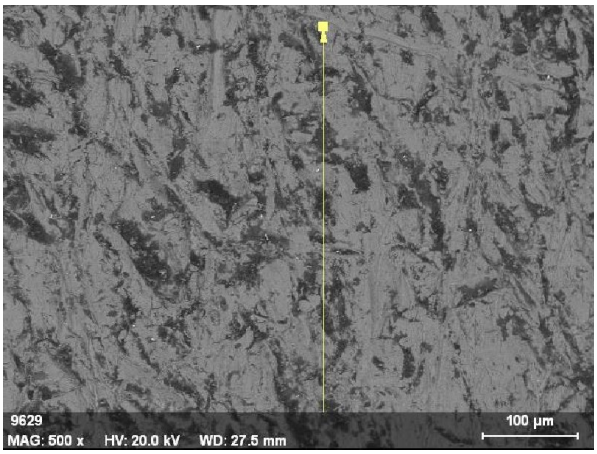

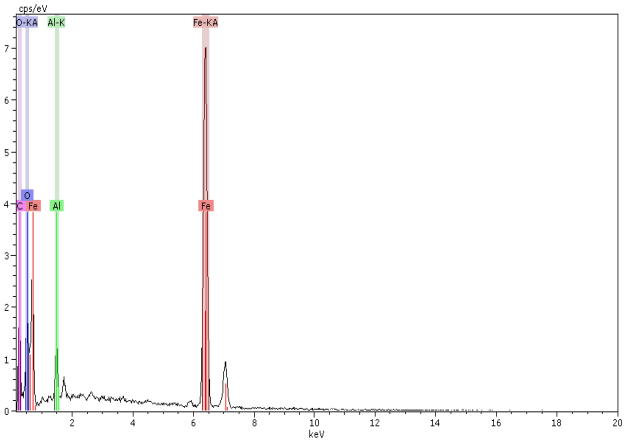

Figure 20. Vertical section microstructure image and chemical analysis of sample B

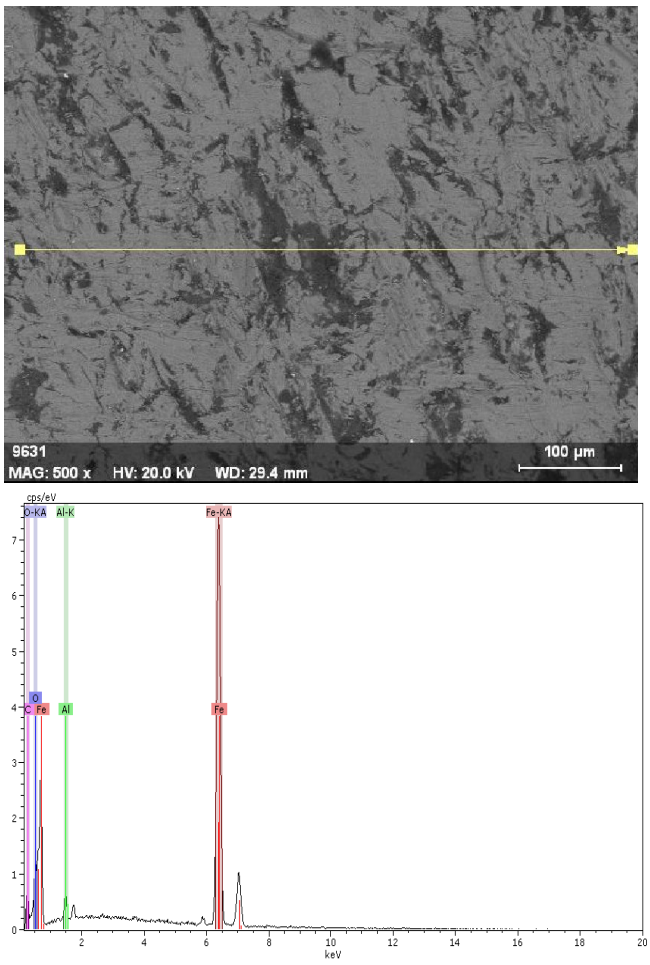

Figure 21. Vertical section microstructure image and chemical analysis of sample C

Finally, the surface of each sample was polished and then the electron microscope image was taken. Their microstructure images are given below.

Figure 22. show the polished surface microstructure analysis of sample A. Figure 23. show the polished surface microstructure analysis of sample B. Figure 24. show the polished surface microstructure analysis of sample C.

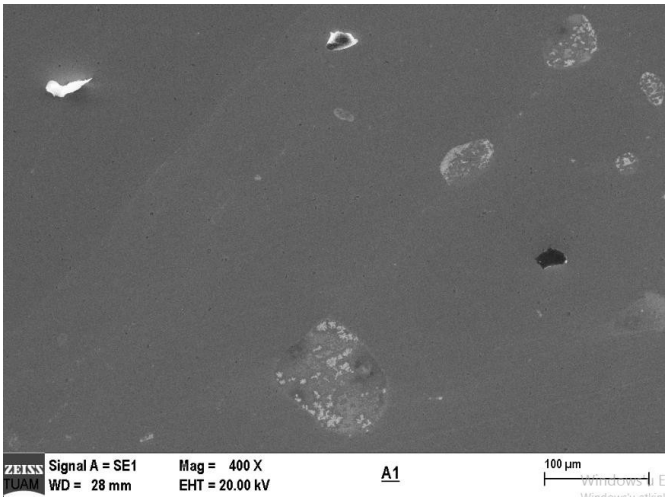

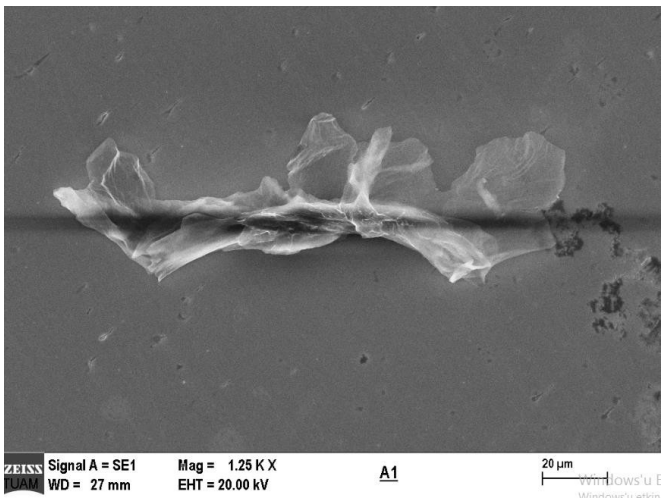

Figure 22. Polished surface microstructure analysis of sample A

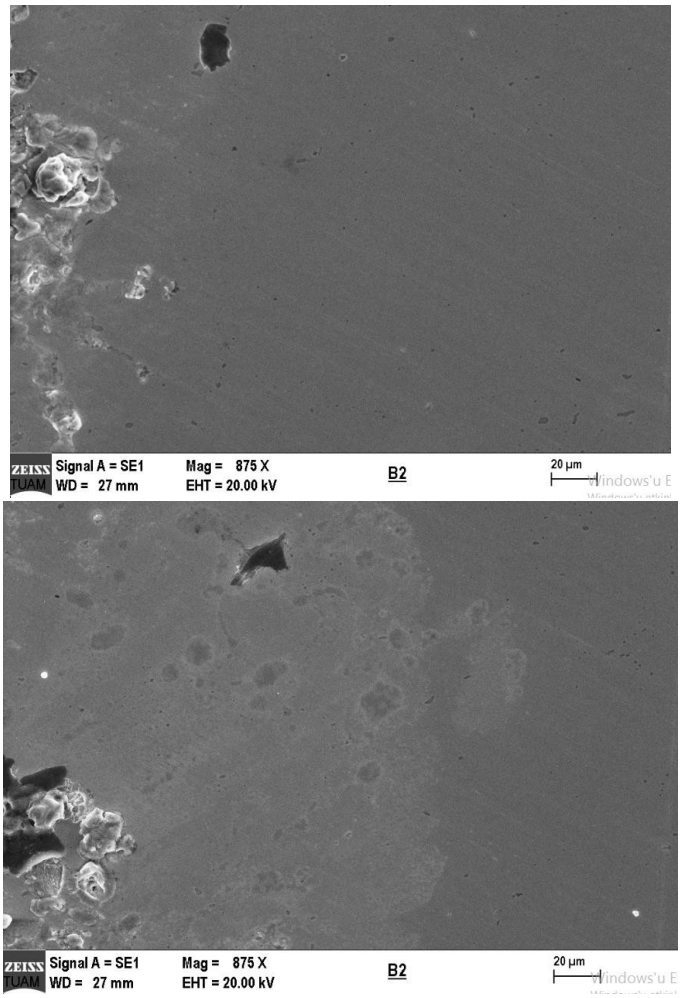

Figure 23. Polished surface microstructure analysis of sample B

doi: https://doi.org/10.26701/ems.477224

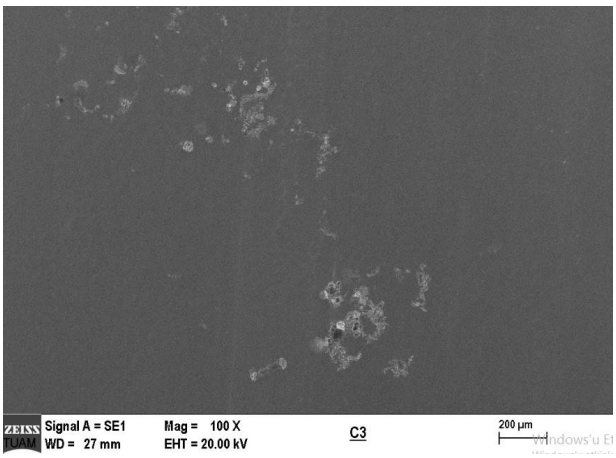

Figure 24. Polished surface microstructure analysis of sample C

3. RESULTS

As a result of the analyzes, all inclusions seen in the parts are solved as a result of optimization of heat treatment parameters as they are in ASTM E45 standards [4]. Trial parameters and results are shown on Table 1.

Table 1. Trial parameters and results

	Original Recipe	Trial 1	Trial 2	Trial 3	Trial 4
Preheating Temperature (°C)	420	420	420	420	450
Carburizing Temperature (°C)	960	960	960	960	960
Boost Cp (%)	1.35	1.35	1.35	1.20	1.20
Boost Time (min)	65	65	65	65	65
Difusion Cp (%)	1.00	0.80	1.00	0.80	1.00
Difusion Time (min)	20	20	20	35	45
Quenching Temperature (°C)	860	820	880	880	880
Soak Time At Quenching Temp. (min)	20	20	20	20	60
Oil Agitators Speed (rpm)	1400	800	1400	1400	1400

TRAIL 1

Purpose: Decreasing the stress of heat treatment step to material.

It's thought that if an amount of stress, which steel with high inclusions can stand, is loaded, there will be no cracks.

Action: Decreasing diffusion Cp to have low amount of martensite, decreasing quenching temperature to have less thermal shock, decreasing oil agitation to have slower cooling rate.

Conclusion: Good hardness values, there are still radial cracks. It is approved that crack is not related with stress which comes from heat treatment step. The cracks after the trail 1 is shown in the Figure 25.

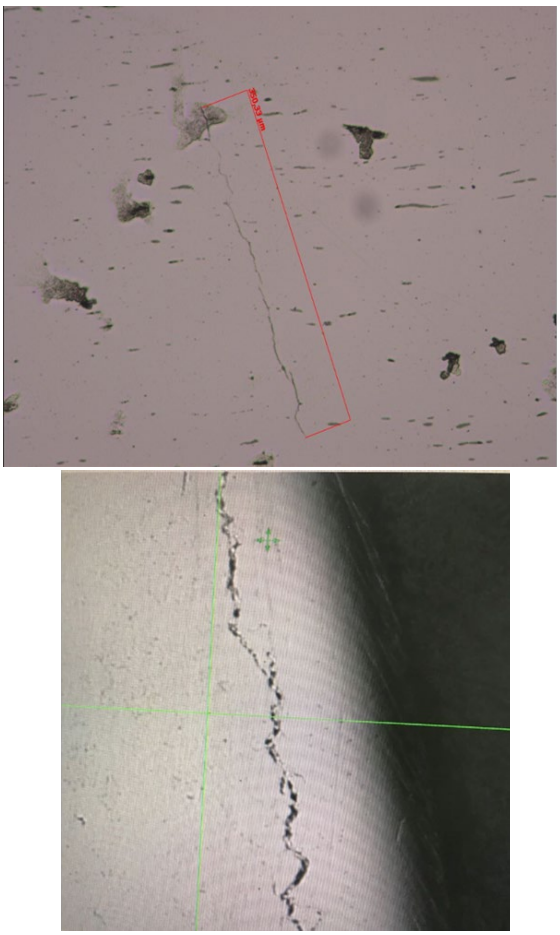

Figure 25. Results of Trial 1

TRAIL 2

Purpose: Decreasing the volume change difference between case and core.

It's thought that if the amount of martensite in the core is increased, there will be less stress gradians between case and core.

Action: Increasing quenching temperature.

Conclusion: Good hardness values, there is no radial cracks, but there are cracks which reach to surface (cylindrical area of pin). The volume change difference idea works. It is evaluated carbides which cause cracks at surface area. The cracks after the trail 2 is shown in the Figure 26.

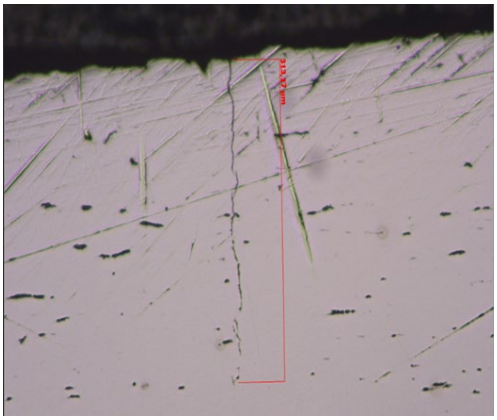

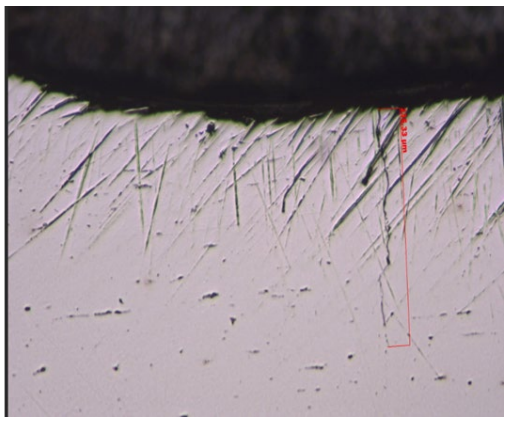

Figure 26. Results of Trial 2

TRAIL 3

Purpose: Getting rid of carbides which cause cracks on grain boundaries.

Action: Decreasing boost Cp, decreasing diffusion Cp, increasing diffusion time.

Conclusion: Good hardness values, there is no radial cracks, but there are still cracks which reach to surface (cylindrical area of pin). Retained austenite decreased below 3%, especially at crack area. It is observed less carbides. The cracks after the trail 3 is shown in the Figure 27.

Figure 27. Results of Trial 3

TRAIL 4

Purpose: Increasing retained austinite to have more elastic case structure, decreasing thermal shocks between preheating and carburizing process, to be sure all parts are at quenching temperature just before quenching step.

Action: Increasing diffusion Cp and time, increasing preheat temperature, decreasing furnace temperature at idle condition, increasing soak time at quenching temperature.

Conclusion: Good hardness values, we don't have any cracks. Retained austenite increased to 8%. The microstructure images observed after the trail 4 are shown in Figure 28.

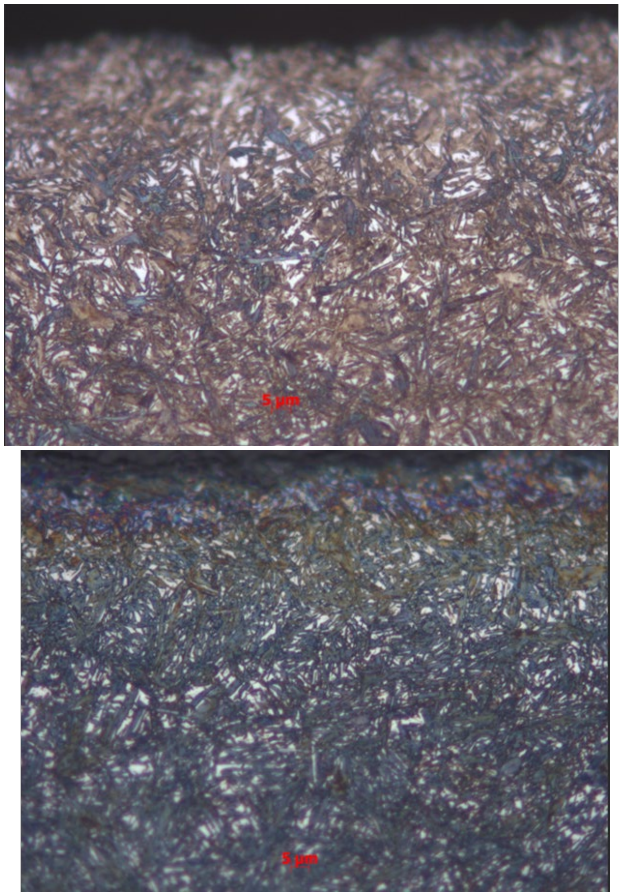

Figure 28. Results of Trial 4

4. CONCLUSION

The micro-structure and chemical analysis of the samples A, B and C and the water-jet specimens are given below.

- All 3 groups (A, B and C) were found to contain variable and similar proportions of superficial voids and inclusion in the sample.
- It is determined that the source of the cavities and inclusions formed in each of the 3 groups are mostly Al, Mn and Si-sourced.
- It is seen that B group samples contain more superficial space (spherical) than other samples.
- In each of the 3 groups, the gap and the inclusion were determined to be at the level of all the other steels and sometimes slightly more (especially at A and C).
- The inclusions and gaps determined in all three samples are thought to originate from the secondary elements entering the structure externally during the shaping of the metal.

- All samples had inclusions and gaps in a non-homogeneous structure. In addition, all 3 samples show a change in shape.
- Polarized microscopy studies in the samples showed fewer coarse grains. In the electron microscope examination, there was more space and inclusion (about 5-10 microns in size), which was small but did not affect the properties. Furthermore, it was observed that linear errors increased in A and C sample as the magnification increased. This is interpreted as the formation of linear grain boundaries during formation of nucleation due to conditions during cooling. Moreover, these linear structures are thought to occur due to different surface energies (properties or contact angles) of the secondary elements in the system.
- Both micro and macro segregation were observed in all samples.
- It is thought that the larger dimensional defects determined in the samples may be caused by the difference in dissolution during casting.

As a result; It is thought that the cavities and inclusions determined in all samples are at a level that will not significantly affect the mechanical or chemical wear, hardness, mechanical friction resistance, elastic modulus, ductility, fracture behaviour and load during operation. In addition, the non-cracking heat treatment parameter was determined from the result of 4 different heat treatment parameters. As a result, the heat treatment parameters have been optimized and the crack problem has been solved.

REFERENCES

[1] "Metallography and Microstructure", Metals Handbook, American Society for Metals, Vol. 9, p. 9, 1985.

[2] C. E. Sims, "Transactions of the Metallurgical Society of AIME", p. 367-393, 1959.

[3] R. Kiessling and N. Lange, "Non-Metallic Inclusions in Steel", Second Edition, Book No. 194, 1978.

[4] ASTM E45-18a, Standard Test Methods for Determining the Inclusion Content of Steel, ASTM International, West Conshohocken, PA, 2018, www.astm.org

EUROPEAN MECHANICAL SCIENCE
e-ISSN: 2587-1110

Research Paper

The Effect of Dolly Suspension Parameters to the European Modular System Vehicle Combination

Enis Gögen*, Koray Emre Özcan

Tırsan Treyler San. ve Tic. A.Ş.

Abstract

The European Modular System (EMS) is introduced to allow increased vehicle length and weight for road freight transport. Directive 96/53EC defines the types of combinations for this modular concept. This study concentrates on the Type-3 EMS so called "road train" including truck, dolly and semi-trailer combination. To get an idea about the effect of this long module combination over the valuable goods transportation, three cases are defined for the dolly's front and rear suspension parameters, than 14-degree of freedom (DOF) half vehicle models are generated in order to observe the dynamic characteristics of the road-train for these three cases. Modal and transient analyses are performed and vertical displacement responses are obtained from front , middle and the end of the semi-trailer's nodal points. Pitch angles of the semi-trailer body are also demonstrated. The change in the bounce responses and the pitch angles are interpreted for all three cases. It is observed that the middle of the body is affected less by vertical displacement.

Key Words : European Modular System, Road Train, Dolly, Half Vehicle Model, Modal Analysis, , Transient Analysis

1.INTRODUCTION

The participation of Sweden and Finland required a new definition for the road freight transport in European Union. As the longer and heavier vehicle combination (LHV) usage is a majority in these two countries, a new modular system is defined with the combination of a 7.82m long swap body and 13.6m long semi-trailer with a total length of 25.25 m called European Modular System (EMS). EMS consists of three modules according to 95/53 EC directive as given in Figure 1. In order to get a 25.25 m long combination, Module A uses a truck/dolly/semi-trailer, Module B uses a tractor/semi-trailer/central axle trailer, Module C uses a tractor/B-train (or B-double) containing swap body/semi-trailer combination.

Several studies have been done to see the advantages and disadvantages of this modular system. In the study of Larsson [1], the benefits of EMS is defined as positive environmental impact over CO_2 emissions, reduced congestion, co-modality & inter-modality, improved traffic safety, supporting logistics efficiently and flexible use of existing vehicle units. Akerman et al. [2] published a study to evaluate the Swedish and Finnish hauliers' experiences. They demonstrate less fuel consumption, reduced transport costs, less vehicles carrying the same amount of properties as the advantages of this concept. They also comment the possibility of increment in the market share of road transports and accident rate as the disadvantages. Whereas Grislis [3] declares that there is not a proven evidence that shows LHVs are more dangerous than an ordinary truck/trailer or truck/semi-trailer combinations. Aurell et al. [4] also mentions LHVs' have better dynamic stability than shorter vehicle combinations. The other benefit of this concept is the intersection with the railway transportation as swap body usage is more popular in road trains. Eom at al. [5] shows shift toward railway from truck presents a sizable opportunity to reduce freight CO_2 emissions.

The aim of the study given in this article is to see the impacts of dolly's suspension system parameters to the general vehicle dynamics for a Module A type combination. In order to see the vehicle responses, a considerable amount of computer simulations are performed. In his Master thesis Lundberg [6] pointed out the importance of the simulation results to understand deeply how several attributes affect the vehicle response as per a particular road excitation.

*Corresponding authour
Email: enis.gogen@tirsan.com

European Mechanical Science, December 2018; 2(4): 128-132
doi: https://doi.org/10.26701/ems.463224
Received: September 24, 2018
Accepted: November 6, 2018

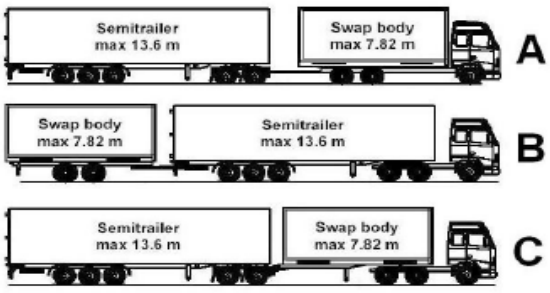

Figure 1. EMS Combinations

to perform modal and transient analyses to see the vertical and pitch responses of the complete vehicle structure. Past literature studies include modal analysis of trailer frames to observe the mode shapes of the complete body [10,11,12]. It can be strongly supported that considering the change in the mode shapes is one of the important design criteria.

Gillespie comments as there are not separate bounce and pitch modes as most vehicles move through the vertical and pitch directions synchronously [13]. Karmiadji [14] performed an analysis including bounce and pitch motions throu-

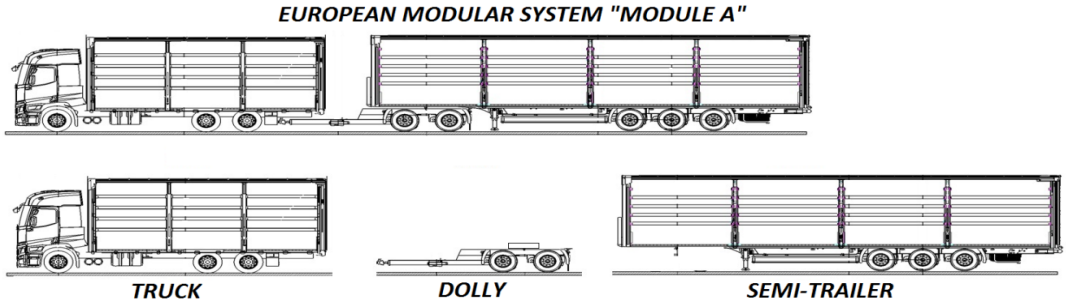

Figure 2. EMS Module A Vehicle Definition

Patil [7] shows the importance of vehicle dynamics models for automotive research and development studies. Several models such as quarter, half and full vehicle models can be used to examine the dynamic behavior of a vehicle. Malgaca et al. [8] uses half vehicle model to observe the bounce-pitch dynamics of a bus, while Philipson et al. [9] mentions using a full vehicle model to see the roll characteristics of a truck-trailer combination.

Figure 3. Dolly Suspension System

In this study three different cases are defined including different suspension parameters and 14-DOF half vehicle models are created for each cases. Half vehicle model is used

gh X-Z body motion algorithm. Penaz et al. [15] made a modal analysis for a three axle semi-trailer, and they also found several pitch-bounce modes. Spivey [16] and Walhekar et al. [17] configured a 15 and 17-DOF half vehicle truck-semi-trailer models respectively to see the dynamic response on several locations of the vehicle combination.

2.METHODS

2.1 EMS "Module A" Vehicle Definition

Complete vehicle combination consists of a three axle truck, two axle dolly and semi-trailer is given in Figure 2. The dolly vehicle includes a telescopic draw bar to supply the connection between the dolly and the truck. The fifth wheel over the dolly let the semi-trailer couples them to each other. Both axles are rigid while the front one is force-steer. Both front and rear suspension systems include an air bellow, trailing arm and hydraulic-telescopic shock absorbers as given in Figure 3.

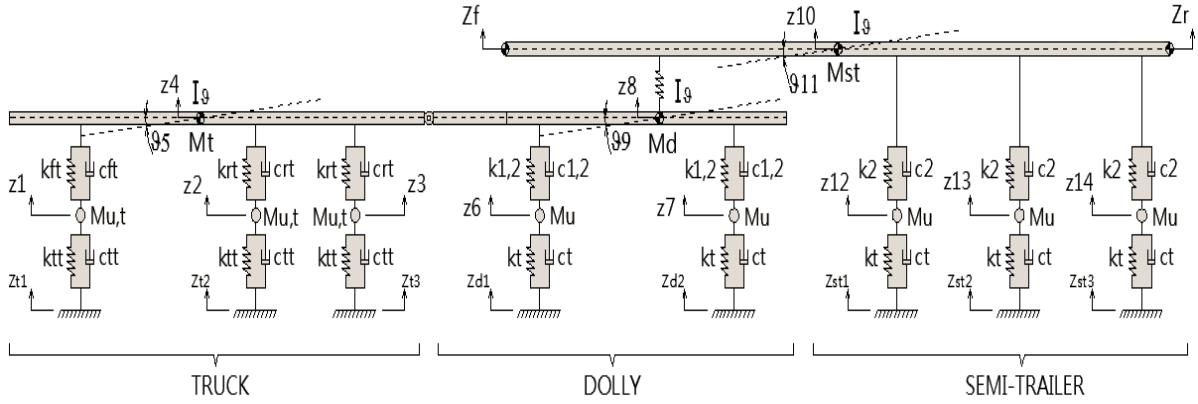

Figure 4. Half Vehicle Model

doi: https://doi.org/10.26701/ems.463224

2.2 Half Vehicle Model and Case Definition

14 degree of freedom half vehicle model is configured as given in Figure 4. System inputs are seen as base excitations zt_n, zd_n and zst_n. System coordinates consists of 11 displacement z_n and 3 angle ϑ_n values. Truck frame, dolly frame and semi-trailer frames are modeled as the solid beam. Unsprung masses are lumped into the wheel centers, $M_{u,t}$ represents the truck unsprung mass and M_u represents the dolly and semi-trailer unsprung masses. Both primary suspension system and tires are modeled with spring-damper couples, spring rate and damping ratios are reduced to wheel axis. There are two different spring and damper characteristics for dolly as given $k_{1,2}$ means k_1 or k_2 which is subjected to soft and harsh springing that will show how the semi-trailer is affected from this parameter changes. Z_f is the front end and Z_r is the rear end vertical displacements of the semi-trailer, Z_{10} is the center of gravity location displacement of the semi-trailer body which is more less in the middle of the frame structure. Continue on of this paper, displacement-time graphics will be demonstrated from Z_f, Z_r and Z_{10} locations for each cases to observe the effect of the suspension parameter change.

As mentioned above there will be 3 different cases as the mixture of two vertical ride frequency values. k_1 and k_2 spring rates will create 1.62 Hz and 2.1 Hz vertical ride frequency, respectively. Table 1 defines the three cases for different front and rear ride frequencies.

Table 1. Case Definition

Case #	Front Vertical Frequency	Rear Vertical Frequency
1	2.1	1.62
2	2.1	2.1
3	1.62	2.1

Table 1 shows that Case 1 represents a harsh front axle springing and a soft rear axle springing, Case 2 represents a harsh springing for both of the axles and Case 3 represents a soft front axle springing and a harsh rear axle springing.

2.3 Modal Analysis

Modal Analyses are performed for all three cases and natural frequency values are given in Table 2. First four mode shapes are belongs to pitch-bounce modes. Malgaca et al. [8] remarked that since the road inputs excide the front wheels of the vehicle first, pitch motions occur even during small obstacle transitions. As a matter of fact it can not be seen a pure bounce or pitch mode in any mode shapes.

In the first mode shape the whole vehicle combination moves together, while the truck and the dolly perform a pitch motion together as a couple, the semi-trailer travels in vertical axis with a very limited pitch motion.

In the second mode shape, the truck and the trailer perform a pitching motion at the same direction but the dolly sweeps a bigger pitch angle. The semi-trailer also pitches harmoniously with the truck and the dolly couple.

Table 2. Natural Frequency Values

Mode Shape #	Case 1	Case 2	Case 3
1	1.49	1.42	1.50
2	1.53	1.53	1.54
3	1.69	1.65	1.71
4	1.78	1.77	1.84
5	10.90		
6	10.94		
7	10.94		
8	10.96		
9	10.97		
10	11.23		
11	11.27		
12	11.77		
13	1640		
14	4947.3		

In the third mode shape, this time dolly and the semi-trailer act as a couple and perform a pitching motion together, while the truck pitches to the other angular direction.

In the forth mode shape, the combined structures move relatively to each other, where the truck and the dolly perform pitch motions to the different angular directions, the situation is the same for the dolly and the semi-trailer, they also pitch to the opposite angular side.

Mode shapes between the fifth mode and the twelfth mode demonstrates the natural frequency modes of unsprung masses of the truck, the dolly and the semi-trailer. Table 2 shows that they are not affected from dolly suspension parameter change.

Thirteenth and fourteenth mode shapes are related with the natural frequency modes of the draw bar coupling and the fifth-wheel coupling respectively. They are also the same for all cases.

2.4 Transient Analysis

Analyses are carried out in ANSYS software including all three cases for the vehicle combination travels over a 0.1m height bump with 54 km/h velocity. Displacement-time graphics are demonstrated in Figures 5, 6 and 7 respectively for three cases including the front end, rear end and center nodal points of the semi-trailer.

3 RESULTS

3.1 Displacement-Time Responses of the Semi-Trailer

Table 3 shows the peak points of the curves for the nodal points according to Figures 5, 6, 7. The maximum displacement values are as given in below table.

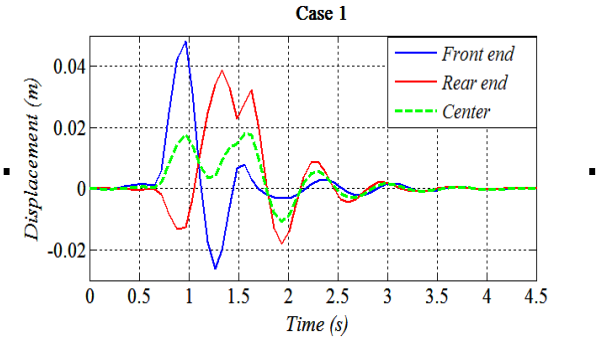

Figure 5. Case 1, Displacement-Time Graphic

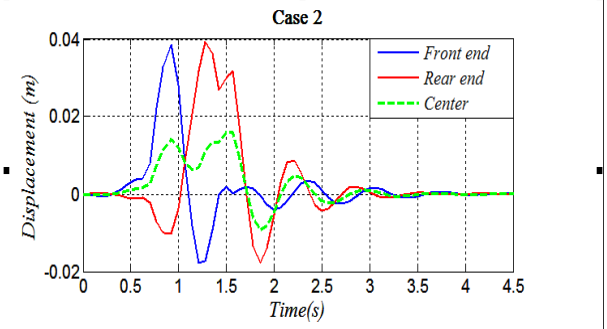

Figure 6. Case 2, Displacement-Time Graphic

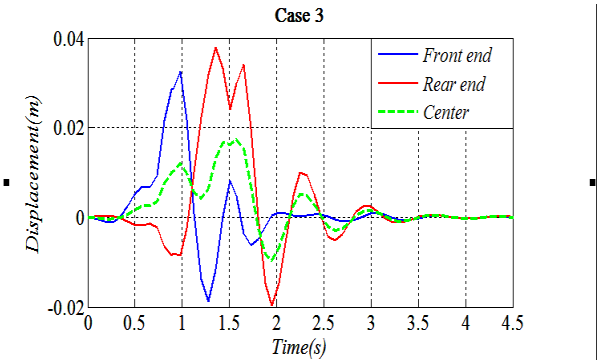

Figure 7. Case 3, Displacement-Time Graphic

Table 3. Maximum Displacement Values

Case #	Travel	Displacement (m)		
		Front end	Rear end	Center
Case 1	Bump	- 0.026	- 0.018	- 0.010
	Rebound	+ 0.048	+ 0.038	+ 0.018
Case 2	Bump	- 0.018	- 0.018	- 0.009
	Rebound	+ 0.039	+ 0.039	+ 0.016
Case 3	Bump	- 0.019	- 0.019	- 0.009
	Rebound	+ 0.032	+ 0.037	+ 0.017

3.2 Pitch Angle-Time Responses of the Semi-Trailer Body

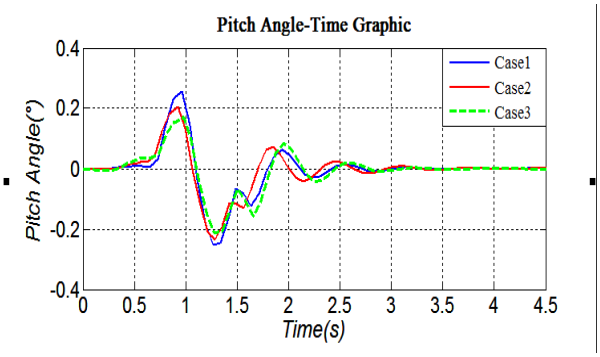

Figure 8. Pitch Angle-Time Graphic

Table 4 shows the peak points of the curves given in Figure 8. The maximum pitch angle values are calculated by the summation of top and bottom angle values.

Table 4. Maximum Pitch Angle Values

Case #	Travel	Pitch Angle (°)
Case 1	Top	0.2548
	Bottom	-0.2518
	Total	0.5066
Case 2	Top	0.2053
	Bottom	-0.2371
	Total	0.4424
Case 3	Top	0.1720
	Bottom	-0.2112
	Total	0.3832

4 CONCLUSIONS

This study analyzed the effect of the suspension parameters change in a dolly to the freight transportation in a semi-trailer.

Modal analysis results show that four mode shapes are effected due to suspension parameter change and all of these mode shapes belongs to pitch-bounce modes. It can be said that there are not a significant change in the natural frequency values with the selected ride frequency cases, but the lowest natural frequency values exist in Case 2 on which both axles have the harsh springing characteristics. Results demonstrate that the increment in the vertical frequency of a suspension system creates a drop in the natural frequency values of the pitch-bounce modes. According to the values given in Table 2, it can be interpreted that if the difference in the vertical frequency values increase between front and rear axles from soft springing through harsh springing, the difference will be more significant in the natural frequency values.

Section 3 demonstrates the nodal responses of the semi-trailer according to the defined cases. Transient analysis results show that maximum front end displacement value occurs in Case 1 which represents a harsh front springing and soft rear springing. Rear end and center nodes seem does not been affected too much from suspension parameters change.

Results given in Table 4 shows that pitch angle is mostly affected from Case 1, harsh front springing and soft rear springing. There is a significant drop in the pitch angle in the semi-trailer body as the springing starts from soft to harsh in the front axle, but the situation is opposite for rear axle springing, if pitch angle is requested to decrease than the rear axle vertical frequency should be increased.

According to the results presented in this study, if a fragile furniture is transported in a semi-trailer of Module A type European Modular System, it will be suggested to be located through the center of the trailer frame as much as possible.

REFERENCES

[1] Larsson, S., (2009). Weight and dimensions of heavy commercial ve-

hicles as established by Directive 96/53/EC and the European Modular System (EMS). Workshop on LHVs Report, Brussels.

[2] Åkerman, I., Jonsson, R. (2007). European Modular System for Road Freight Transport. Experiences and Possibilities. Report 2007:2 E. Stockholm: TFK – TransportForsk AB. 91 p.

[3] Grislis, A. (2011). Longer Combination Vehicles and Road Safety. Transport. 25(3):336-443

[4] Aurell, J., Wadman, T. (2007). Vehicle Combinations Based on the Modular Concept: Background and Analysis. Report No 1/2007. Committee 54: Vehicles and Transports. Sweden : Nordiska Vägtekniska Förbundet (NVF). 64 p.

[5] Eom, J., Schipper L., Thompson L. (2012).We keep on truckin':Trends in freight energy use and carbon emissions in 11 IEA countries. Energy Policy. 45:327-341

[6] Lundberg, T. (2013). Analysis of simplified dynamic truck models for parameter evaluation. Department of Aeronautical and Vehicle Engineering KTH Royal Institute of Technology. Master Thesis. ISSN 1651-7660.

[7] Patil, V. (2017). Generic and complete vehicle dynamic models for open-source platforms. Department of Mechanical, Maritime and Material Engineering, Process and Energy, TU Delft, Netherlands. Master Thesis.

[8] Malgaca, L., Gögen, E. (2015). The Effect of Front and Rear Ride Rate Ratios to the Pitch Angle of a Midibus. International Journal of Natural and Engineering Sciences. 9(1):44-48. ISSN:1307-1149, E-ISSN:2146-0086.

[9] Philipson, N., Andreasson, J., Gafvert, M., Woodruff, A. (2008). Heavy Vehicles Modeling with the Vehicle Dynamics Library. Modelica. Lund, Sweden.

[10] Sharma, D., Vora, Y.D. (2017). Design and Vibration Analysis of Heavy Duty Vehicle (Trailer) Chassis Through FEM Software. International Journal of Engineering Science Invention Research & Development. 3(11). e-ISSN:2349-6185.

[11] Lian, K., Fan, B., Miao, Y., Zhu, X. (2016). Research on Optimal Design and Modal Analysis of the Frame. International Conference on Artificial Intelligence:Technologies and Applications (ICAITA 2016). p:272-274.

[12] Mahmoodi-k, M., Davoodabadi, I., Visnjic, V., Afkar, A. (2014). Stress and Dynamic Analysis of Optimized Trailer Chassis. Technical Gazette 21. 3(2014):599-608.

[13] Gillespie, T. (1992). Fundementals of Vehicle Dynamics. Society of Automotive Engineering. Warrandale, PA.

[14] Karmiadji, D.W. (2005). Analyzing the Bounce and Pitch Phenomenon of Vehicle Model Through XZBM Algorithm. Jurnal Ilmiah Semesta Teknika. 8(2):137-145.

[15] Penaz, J., Voltr, O. (2013). Dynamic Analysis of Behaviour of Three-axle Semi-trailer Road Tank Going on Special Waved Roadway. Transportation Engineering.41(2):139-142.

[16] Spivey, C. (2007). Analysis of Ride Quality of Tractor Semi-Trailer. Department of Mechanical Engineering, Clemson University. Master Thesis.

[17] Walhekar, S.B., Burande, D.H. (2015). Modeling of 17-DOF Tractor Semi-Trailer Vehicle. International Engineering Research Journal (IERJ). 2:5089-5093. ISSN:2395-1621.

EUROPEAN MECHANICAL SCIENCE
e-ISSN: 2587-1110

Research Paper

Insulated Patient Transport Capsule for Chemical, Biological, Radiological and Nuclear (CBRN) Contamination Cases

Ferit İşbilir, M. Fahri Kaynak*, M. A. Alparslan Kesemen

Ems Mobile Systems Inc. Ankara, 06935, Turkey

Abstract

CBRN is used as an abbreviation for the chemical, biological, radiological and nuclear word group. In general, this term refers to hazardous and dangerous situations that are caused by chemical, nuclear, biological and radioactive materials which can be spread intentionally or accidentally causing harm to humans and the environment. Developments in technology, disasters, accidents, war or terrorist events all enhance the risk of CBRN at the present time. These risks can cause situations that can directly threaten the lives of large amounts of people and cause many people to lose their lives or can result in significant life changes for people affected. CBRN risky events cause panic and disorder in society. Most importantly, people who interfere in these events are at great risk like people who are exposed. In this study, working principle, functions and capsule analysis and tests of the insulated patient transport capsule, developed in order to protect both the environment and the interveners in CBRN events were examined. If we think about our country's geopolitical position or regional geography, an isolated patient transportation capsule is a critical life-saving product both at military and civil level. The negative pressure, generated in the capsule protects the environment and interferers from CBRN contamination. It provides treatment and an emergency response opportunity with protective gloves and sealed ports for serum on the capsule as well. The isolated patient transport capsule can be placed on the stretcher with connection apparatus and easily transported.

Keywords: CBRN, Insulated patient transport, Capsule

INTRODUCTION

CBRN is used as an abbreviation for the chemical, biological, radiological and nuclear word group. In general, this term refers to hazardous and dangerous situations that are caused by chemical, nuclear, biological and radioactive materials which can be spread intentionally or accidentally causing harm to humans and the environment (1). CBRN events are undesirable, and when they are experienced they are very difficult events which have a big impact. These events cause panic and disturbance. For example; Ebola outbreak occurred in 2014 and it caused a serious panic in Turkey and all the World. The intervention in these events is difficult and time-consuming because the interventionist is at risk and there is a possibility of transmission of CBRN substances. For this reason, personal protective equipment is required for the handling of these materials.

The Ministry of Health published the Ebola Virus Disease Case Management Guide in 2015 which contained information on the detection, control and treatment of the disease. Underneath the emergency service approach algorithm title, the issue was mentioned about the transfer of the patient and how to intervene in emergency situations. During the transport of such patients, the equipment to be available in ambulances is listed. These equipment's includes gloves (double gloves), liquid impermeable apron, liquid impermeable overalls, safety glasses, face shield / shield, protective headgear-hat (no headgear cap), N95 / FFP3 mask, waterproof foot protector and alcohol-based hand sanitizer (2). As it can be seen, each of the events of CBRN is a heavy burden on health services. It is necessary to be prepared as well. It is essential for our country to be prepared for risky events which are possible due to its geopolitical position and the events in the surrounding geographies. By isolating the patient, the risk of exposure to the environment will be prevented during transport. Transport of the exposed person to the health center will be easy and safe. At the same time, with the use of the insulated patient transport capsule, personal protective equipment will be used at minimum level.

In this study on the insulated patient transport capsule,

*Corresponding authour
Email: fkaynak@ems.tc

European Mechanical Science, December 2018; 2(4): 133-139
doi: https://doi.org/10.26701/ems.464243
Received: September 26, 2018
Accepted: November 27, 2018

considerations regarding the design of the capsule and the design considerations, the filtering system, the functions of the negative and positive pressure in the capsule and how to generate it, the air flow dynamics in the capsule and the tests to be applied to the capsule are included.

1. General Information About CBRN

CBRN refers to hazardous and dangerous situations that are caused by chemical, nuclear, biological and radioactive materials which spreading to intentional or accidental ways for the humans and the environment (Ebola Vaka Yönetim Rehberi, 2015).

CBRN events are undesirable, but when they are experienced they are very difficult events and impacts. In order to minimize and control the effects of these events, it is necessary to know what the terms are related to CBRN.

1.1. Terms Related To CBRN

Chemical Threat: In industrial applications, chemical substances are used as raw materials or intermediates, and in domestic use, cleaning or daily maintenance is widely used. In parallel with the development of the chemical industry, the usage of these substances is increasing day by day. This increase brings with it some threats. Accidents occurring in organized industrial zones and producing, processing or storing chemicals will affect people and the environment negatively.

In recent years, it has been discovered that these substances can be used to harm specific targets as a result of the studies on waste chemicals. Increasing the effects of waste chemicals by changing their structures has caused these substances to become potential weapons. Hence, chemicals have been used in terrorist acts and wars (3).

Biological Threat: Biological threats; all of the threats consist of conditions such as biological agents and unsafe laboratory procedures. This definition; natural biological diseases (non-infectious and non-infectious), environment or animals identified, biological agents that are likely to infect humans, biological agents that contain or emit biological weapons (biological weapons), the terrorist attacks with biological agents (bioterrorism) (4).

Radiological Threat: Radiological events are events in which the public is exposed to radiation or radioactive material for certain reasons. Transport of radiation sources and their use in applications, lost and stolen resources, possible sources of scrap, fire with hardware and planning errors, disasters such as earthquakes can cause radiological events (5).

Nuclear Threat: Used to both benefit from the occurred energy of fragmentation (fission) of nuclear materials (uranium, plutonium, etc.) or the combination of two atoms(-fusion) expresses the destructive pressure wave, lethal radiation, and high heat. A nuclear explosion; is an explosion which occurs a strong light, a wave of heat and pressure show up and the propagation of radioactive substances that contaminate air, water and surfaces (6).

Contamination: CBRN is the transmission of substances to personnel, land, materials, equipment and foodstuffs (7).

Decontamination: It is the process of removing the chemical substance from all contaminated by specially trained people using special equipment and solutions (7).

1.2 National and International Organizations Related to CBRN

As international organizations on the subject of CBRN, International Atomic Energy Agency (UAEA), International Radiation Protection Committee (ICRP), European Atomic Energy Community (Euratom), European Center for Nuclear Research (CERN), Nuclear Suppliers Group (NTG) and Zangger Committee are actives.

Regarding the issue of CBRN and the control and intervention of CBRN events in our country, Turkey Atomic Energy Agency (TAEK), Turkish Armed Forces, Public Health Presidency, Disaster and Emergency Management Presidency, Turkish Red Crescent and Organizations such as the National Poison Center (UZEM) are operating (8).

1.3 Events Related to CBRN

There have been many events in history related to the subject of CBRN. Many people have lost their lives in these events. In fact, in the long term after the events have been found to have consequences that will affect human life. There have been many incidents for each threat identified in Article 1.1. Some of the recent events are given below.

The chemical weapons attacks in Syria in August 2013 caused the deaths of more than 1000 people, including women and children. (Chemical)

In the United States in the weeks following the September 11 attacks, anthrax mail sent to different institutions caused 22 people to be infected in total and 5 people died (Biological)

In 2011, after the magnitude 9 earthquake in Töhoku and the tsunami in Japan, to an accident at a nuclear power plant in the Fukushima area caused a large amount of radiation. (Radiological)

In 1986, a large amount of radioactivity leaked into the environment due to an accident in a nuclear power reactor in the Chernobyl region of Ukraine. (Nuclear) (9).

2. Insulated Patient Transport Capsule

The insulated patient transport capsule, an area contaminated with CBRN agents, primarily affects people of these substances leads to transfer to the center where they are treated, is a mobile patient transport capsule.

This capsule also has features for the user to provide a safe medical intervention to the person in the capsule by means of the ports on it. In addition, the capsule can be placed on the stretchers in the ambulances by means of the connection

apparatuses on it so that they can be carried easily. It can provide safe transportation with plane, ship and any vehicle independent stretcher. The solid structure which provides isolation in the capsule is resistant to bad fact such as falling and impact. It allows up to 120 kg. The design of the capsule, filtering and pressure generation system, analysis in capsules and tests are explained in the sub-headings.

2.1. Design of The Insulated Patient Transport Capsule

During the design process, The personnel who will use the capsule and the situation of persons exposed to CBRN that will be in the capsule are taken into consideration. Consultations with persons who have knowledge about CBRN and who have worked in this field previously (AFAD and TSK officials) have introduced the requirements.

CBRN disaster is almost most frightning incident in the World. The people who affect to cbrn agent, are shock and feeling insecure. These factors are most important to design process for us.

In the design of the capsule, it is aimed to instill the psychology of the people in the capsule in a safe place and to heal. Hence the design is shaped around trust, protectionist and color keywords.

We predict The people who affect CBRN agents have a problem with trust. Therefore, we choose first and main keyword as trust. It is emphasized that the human psychology and design can be handled both and we decided to abstract design to factor commanly.

It is aimed to make people feel more secure and to feel that they are in a sheltered place.

One of the most important considerations in the design has been the colors. Each color has a different characteristic and each color causes different emotions in human perception. Which colors to use when starting design is also an important element. Research shows that colors affect the psychology of people. For example; according to research yellow colors gives a sense of temporality. Blue and shades are used in design by considering this principle. According to research blue and shades indicate calmness (10). In other words, blue is a calming color, and even in some European countries, the bridge railings are painted blue to reduce suicides due to the calming effect of blue. In addition, according to research, the blue color represents trust and the purity of blue gives a protectionist psychological effect. In this context, R-171, G-236, B-255 color codes are used.

Considering the human psychology within the capsule, it is decided to use simpler and softer lines instead of the lines that would be perceived by the human eye as complex in design. In the same way, it is paid attention to symmetry in order to make people in the capsule feel safe.

In the design of the capsule, care was taken to ensure that the person within the capsule had the field of vision. People feel more confident in what they see. For example, people would rather travel in the place where they can see every place instead of traveling in an enclosed space. This situation reveals confidently and controlled perception in the subconscious of people. Considering this aspect of the design, attention was also paid to the issue of refreshment, especially considering that the capsule could be perceived as a coffin.

Fans generate negative and positive pressure in the capsule are designed as far from the people in the capsule as possible to minimize the damaging potential of patients who have difficulty in self-control.

The designed capsule is mainly composed of components in Figure-1.

Figure 2 shows the three-dimensional view of the capsule from different perspectives.

Figure 3 shows a picture describing the using of the capsule.

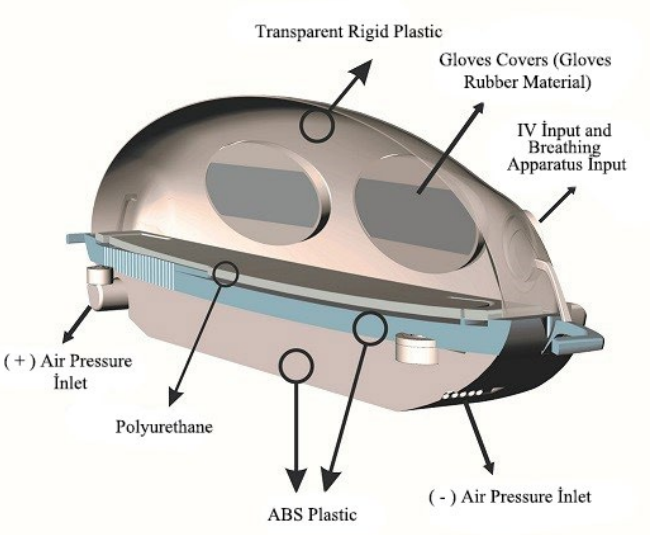

Figure 1- Basic components of the insulated patient transport capsule

Figure 2- 3D design of the insulated patient transport capsule

doi: https://doi.org/10.26701/ems.464243

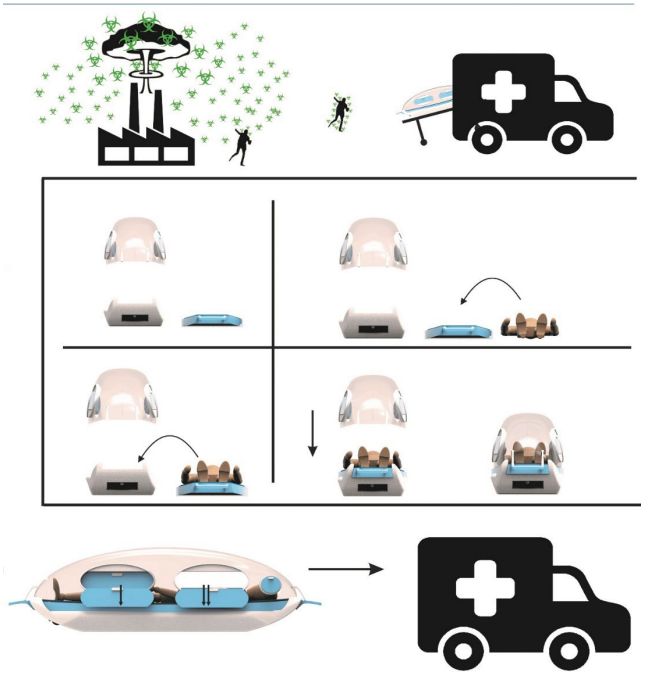

Figure 3-Use of the insulated patient transport capsule

As can be seen from Figure 3, there are caps on the capsule that provide intervention to the patient. With the help of protective gloves that are ready in these caps, to the patient is intervened when necessary. These covers are designed to provide sealing.

In addition, when the capsule is used in conjunction with the stretcher, areas, where medical devices such as ventilators and defibrillators can be mounted in vital situations were also designed.

2.2. Working Method of Isolated Patient Transport Capsule

Negative and positive pressure can be generated depending on the conditions inside of the insulated patient transport capsule. When negative pressure is generated inside of the capsule, as shown in Figure-4, the contaminated air because of the person who exposed to CBRN cleaned by the help of filters discharges outside of the capsule and protects the environment.

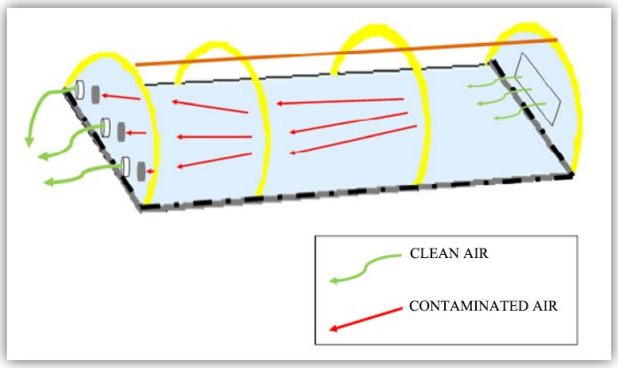

Figure 4- Working principle of the capsule with negative pressure

The pressure inside of the capsule is carried out by the help of two fans. One of these fans is generated positive and the other is negative. Positive pressure works like intensive care logic of hospitals for protects the patient from the external environment. Each one of fans has a separate control unit and the fans can control by the help of these units. The pipe and valve system coming out of the fans pass through the filters and generate pressure inside of the capsule.

The negative or positive pressure values in the capsule can be up to 30 Pascal and these values can be adjusted via the control unit.

The fan system can operate nonstop for 3 hours through to the designed power system and this power system is fully charged for a period of 5 hours.

the HEPA filter system and the ventilation system that clean the contaminated air are found in the capsule. The design of these filters is designed according to the ports formed on the capsule and is in the form of cylindrical.

Laboratories which studies microorganism are carried out are classified as 4 levels according to danger situations. Laboratories which studied on the spreading of avian influenza in aerosol form and microorganisms such as sars and anthrax are defined as BSL3 levels at the High-risk. at the BSL3 clean rooms should be the ventilation system that is single pass recirculation according to TS 11605. The discharged air is cleaned by high-efficiency HEPA filters.

There are pressure, temperature and humidity indicators on the capsule, to inform about the inside of the capsule to the user, who is using the isolated patient transport capsule. With the help of these indicators, the person who is in the capsule can be monitored and taken measures for the necessary situations.

2.3. Analyses of Isolated Patient Transport Capsule

In the insulated patient transport capsule, it is a technical obligation that the interior space is small and that the protective gloves are in the direction of the targeted air flow corridor.

As the HEPA filter efficiency is directly related to geometrical sizing, the geometric design of the capsule was first performed. The 3D model designed in Solidworks was checked for their suitability by testing by selecting HEPA filters which provide the desired parameters at the end of the geometric design.

Hygienic minimum fresh air flow rate in hospitals, at the intensive care unit (for patients with infection and transport hazard) is determined as 30 m^3 / hour. Although the volume in the capsule is not as much as an intensive care unit, this criterion is taken as reference for the purpose of maximizing efficiency. The internal volume of the capsule is 0.58 m^3 and it is considered as 1 m^3 in calculations and fan selection. In this case, an air flow rate of 30 m^3 was calculated to need in the capsule.

In the insulated patient transport capsule, air flow in the capsule was modeled using computational fluid dynamics (CFD) technique to determine the presence of stagnant zo-

nes without air flow. ANSYS software was used to carry out this technique. ANSYS is a general-purpose software, used to simulate interactions, physics, structural, vibration, fluid dynamics, heat transfer and electromagnetic for engineers. The air flow distribution into the capsule was analyzed in the turbulent flow conditions. The time-dependent continuity and momentum equations for analysis were solved. Turbulent flow is defined by the k-ε model. Finite volumes method is used in numerical solution of flow equations. In the analysis, a digital network consisting of approximately 1.5 million triangular pyramid elements was used. The boundary conditions of geometry have been chosen to represent the physical structure and flow dynamics of the capsule in a realistic manner. The geometry of the insulated patient transport capsule was modeled to partially simplified in order to keep the calculation cost of flow analysis reasonable.

After modeling, analyzes were started. The flow distribution around the inlet from the fans through the pipe is given in Figure-5. There are relatively high speeds at near the pipe inlet is mentioned.

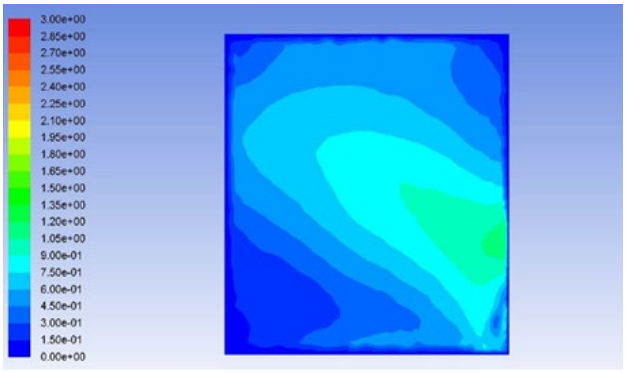

Figure 5 - Flow Distribution (Space Around the Pipe Entry)

In the capsule, flow rates were generally observed to be over 0.2 m / s. As seen in Figure-6 shows, there is no any a stagnant region of air flow.

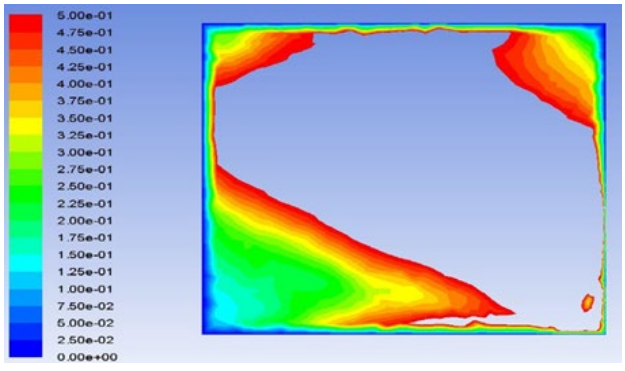

Figure 6- General air flow distributions in the capsule

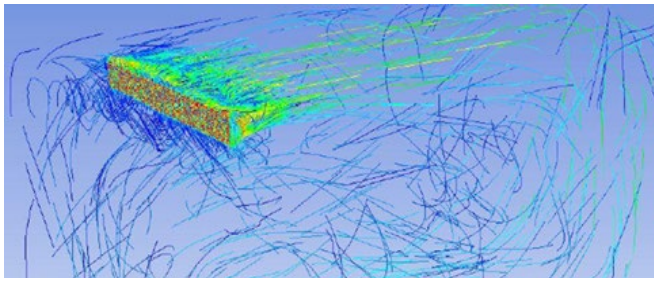

Figure 7- Velocity flow lines in the capsule

In Figure-7, the velocity flow lines are shown as a result of the CFD analysis of the capsule.

As a result of CFD analysis, it was found that there was generally no stagnant area in the capsule and the air flow was efficient.

2.4. Tests Applied to Isolated Patient Transport Capsule

In the insulated patient transport capsule, the following tests were carried out to check the operation of the system as well as to verify the studies such as design and analysis.

2.4.1. HEPA Filter Impermeability Test (IEST-RP-CC034.2: 2005)

In the HEPA filter system contained in the capsule, two 100x100 mm / H 13 HEPA filters were tested with PAO (suppressed aerosol smoke generated by heat evaporation of mineral oils). The HEPA filter and the permeability test of the HEPA filters nests have been successfully completed.

2.4.2. Air Flow and Flow Measurement

The purpose of this test is to understand that the performance of the fan system in the insulated patient transport capsule does not deviate from the desired performance values due to HEPA filters and pressure changes. Therefore, the total number of air changes in the test was calculated. As an evaluation criterion EU / GMP Volume 4 Annex: 1 2008 CGMP / FDA-Din 1946/4: 2008 is taken as reference and the measurement results are in accordance with TS EN ISO 14644/1 ISO 5 class and the results are given in Table 1.

Table *1- Air Flow and Flow Measurement*

ROOM	AMOUNT OF THE AIR SUPPLIED (m^3/h)	AMOUNT OF THE FRESH AIR (m^3/h)	AIR EXCHANGE NUMBER (times/h)	ACCEPTABİLİTY CRITERIA (times/h)	RESULT
Fans	36	0	35	30	Ok
Hepa Filter-1	15	15	5	3	Ok
Hepa Filter-2	15	15	5	3	Ok

2.4.3. Difference Pressure Measurement and Air Flow Aspects

Pressure difference and air flow direction in the insulated patient transport capsule measured according to IEST-RP-CC012.2 and EU / GMP Volume 4 Annex: 1 2008 as well as the religion standards 1946/4: 2008.

The air flow directions (for negative pressure condition) should be from the outside air to inside the capsule. This is because the dirty air caused by the person with the CBRN element does not go out of the capsule. The septic (BSL-4) areas related to the pressure flow directions will be inward negative.

Table *2 - Difference pressure measurement results*

Name of the Room	Air Flow Direction	Room Class	Compare of Field	Measured Pressure	Acceptability Criteria	Result
Insulated patient transport capsule	Left to right	BSL-4	External Environment	-34 Pascal	Greater than (-30) Pascal (Absolute Value)	Ok

doi: https://doi.org/10.26701/ems.464243

The measurements are given in Table 2 and the results are appropriate.

2.4.4. Particle Count and Room Classification

At the measurement points, the 95% upper-reliability limitation at the clean room, counting of the particles have done according to ISO 14644-1 and EU/GMP Volume 4 Annex:1 2008.

The measurement results are in accordance with the TS EN ISO 14644/1 ISO 5 criteria. ISO 5 class particle numbers were determined in 7.3 in the article. Measurements and results are given in Table 3.

Table *3*- Particle counting and measurements of isolated patient transport capsule

Name of Room	Total Particle Counting Point	GÜS (UCL) % 95 0,3 mm/CM	GÜS (UCL) % 95 0,3 mm/CM	Conditions	Result
Insulated Patient Transport Capsule	3	6,559	1,706	No patient	Ok
		Average	Average	At Rest	

2.4.5. Decontamination Time Tests

At the measurement points, the 95% upper-reliability limitation at the clean room, counting of the particles have done according to ISO 14644-1 and EU/GMP Volume 4 Annex:1 2008. The measurements were evaluated according to the decontamination time. The duration of decontamination is the time to decrease to the level of ISO Class 5 after polluting the air in the insulated patient transport capsule.

The measurement results are in accordance with TS EN ISO 14644/1 ISO 5 class. ISO 5 class features were determined in 7.3 in the standart.

3. Findings and Discussion

The following conclusions are given below about to researches about the methods used for the intervention of the CBRN events and the transfer of the people exposed to these events to the related centers.

A scientific publication in the United States deals with the emergency aid process for an Ebola patient. In this study, all the surfaces in the ambulance, including medical devices in the ambulance, were covered with a 6 mm thick plastic film during the patient's transplantation. Similarly, "the named Prevention and Decontamination of Chemical, Biological, Radiological and Nuclear Pollutants for Emergency Medical Personnel During Ambulance Services" published in South Korea was taken into consideration and all surfaces of ambulance were covered with plastic film (11). With this application, it is aimed to protect those who intervene in CBRN events. In this article, don't need to cover the ambulance with the plastic film while an insulated patient carrying capsule is using. The capsule can generate negative pressure as a method of working and consequently the environment and the interveners are protected. Moreover, the impermeable ports on the capsule also allow emergency intervention to the person exposed to CBRN.

There are some patient transport cabins developed around the world to be used in CBRN events. The common feature in these cabins, including the products of the companies that sell these products as distributors in our country, is the material used for isolation tent format. Insulated patient carrying capsule provides isolation with solid plastic. Tent type material has lightness, foldability aspects advantageous. It is also at great risk in terms of deformation and tearing conditions. In case of a possible tearing, the isolation function will be disabled, and the environment and those who intervene will be at great risk. Also, the tent format is less likely to protect the patient in cases such as falls. For isolation in the insulated patient carrying capsule, the use of a solid material is very safe both in terms of deformation and fall.

Conclusion And Recommendations

CBRN events are undesirable, but when they are experienced they are very difficult events and impacts. These events cause panic and disorder. For example; The Chernobyl Incident that took place in 1986 affected almost all of the Black Sea region in our country. Intervention in CBRN events is difficult and time consuming. Because the first responder is at risk and there is a possibility of transmission of CBRN substances. For this reason, personal protective equipment requires the use of materials.

The insulated patient transport capsule provides rapid intervention to those exposed to the CBRN risk events, ensuring that the interveners are exposed to the same risk at the minimum level. Thanks to the isolation, the risk of exposure is prevented from spreading to the environment during transportation and the transport of the exposed person to the health center becomes easy and safe. The insulated patient carrying capsule and personal protective equipment are used at a minimum level, and as described in the findings and discussion section, ambulances that do not require special equipment arise.

In this study on the insulated patient transport capsule, the design of the capsule and the considerations in the design, the filtering system, the functions of the negative and positive pressure in the capsule and how to generate them, the air flow dynamics in the capsule and the tests applied to the capsule were examined. The capsule successfully completed the tests. The CBRN is also looking for people who are exposed to CBRN and hospitals.

The insulated patient carrying capsule is designed to be compatible with the manufacturer's existing stretchers used in ambulances. Developing the connection adapters, which will enable the capsule to work in harmony with other stretcher groups, will promote the use of the capsule, CBRN events will be more effective.

REFERENCES

[1] https://www.afad.gov.tr/tr/23793/KBRN-Sozlugu?kelime=KBRN accessed on 9 September 2018.

[2] T.C. Sağlık Bakanlığı Türkiye Halk Sağlığı Kurumu. (2015). Ebola Vaka Yönetim Rehberi Ankara.

[3] https://www.afad.gov.tr/tr/23667/Kimyasal-Tehditler accessed on 10 September 2018.

[4] https://www.afad.gov.tr/tr/23683/Biyolojik-Tehditler accessed on 10 September 2018.

[5] https://www.afad.gov.tr/tr/23703/Radyolojik-Tehditler accessed on 10 September 2018.

[6] https://www.afad.gov.tr/tr/23740/Nukleer-Tehditler accessed on 10 September 2018.

[7] Sağlık Bilimleri Üniversitesi Gülhane Sağlık Meslek Yüksekokulu. (2017). Kimyasal Biyolojik Radyoaktif ve Nükleer (KBRN) Olayları Ankara.

[8] T.C. Millî Eğitim Bakanlığı. (2017). Kimyasal Biyolojik Radyasyon Ve Nükleer (Kbrn) Tehlikelerde Acil Yardım Rize.

[9] Millî Eğitim Bakanlığı. (2011). Kimyasal biyolojik radyasyon ve nükleer (kbrn) tehlikelerde acil yardım. Ankara: Devlet Basımevi.

[10] Kıran, A.,1986, "Rengin Psikolojik Etkilerinin İncelenmesi ve Deneysel Psikoloji Yöntemi İle Ülkemiz İçin 18-25 Yaş Üzerinde Renk Tercihlerinin Saptanması", Doktora Tezi, İstanbul

[11] Lowe J. J., Jelden K. C., Schenarts P. J., Rupp L. E. Jr., Hawes K. J., Tysor B. M., Swansiger R.G., Schwedhelm S. S., Smith P.W. & Gibbs S.G. (2014). Considerations For Safe Ems Transport Of Patients İnfected With Ebola Virus, Prehospital Emergency Care,1–5.

EUROPEAN MECHANICAL SCIENCE
e-ISSN: 2587-1110

Research Paper

Influence of the Composition on the Exploitation Properties of Combined Medium Density Fibreboards Manufactured with Coniferous Wood Residues

Petar Antov[1*], Viktor Savov[2], Nikolay Neykov[3]

[1,2]Department of Mechanical Technology of Wood, Faculty of Forest Industry; University of Forestry - Sofia, 10 Kliment Ohridski Blvd., 1797 Sofia, Bulgaria
[3]Department of Management of Natural Resources, University of Forestry - Sofia, 10 Kliment Ohridski Blvd., 1797 Sofia, Bulgaria
ORCID: V. Savov (0000-0001-5111-8760)

Abstract

One of the main disadvantages of medium density fibreboards (MDF) in comparison with particleboards is the higher price of the panels, due to the energy-intensive defibration process.
Studies on the possibilities for replacing a part of the wood fibre mass in the composition of MDF with coniferous sawmill residues (shavings) obtained from bandsaw, are presented in this article. The experimental plan is designed using the McLean and Anderson method for studying the properties of multi-component systems in the presence of constraints on the components. The content of coniferous wood shavings varies up to 40%. The panels are manufactured with a density of 720 kg.m^{-3}. The content of urea-formaldehyde resin varies from 8 to 14% in order to compensate the negative effect of the inclusion of coniferous wood shavings in the composition of the manufactured MDF panels. The main exploitation properties of the panels are determined. Experimental and statistical models on the influence of the studied factors are obtained by applying stepwise regression and optimization is performed in order to acquire the best exploitation properties of MDF panels.
As a result of the study it was determined that in order to achieve the values of MDF properties, required by the respective standards, the maximum permissible content of coniferous wood shavings should be up to 10.6%, in which case the content of urea-formaldehyde resin should be above 10%. If the content of urea-formaldehyde resin is below 10%, the maximum permissible content of coniferous wood shavings should be up to 5%.

Keywords: medium-density fibreboards (MDF), wood fibre mass, coniferous wood residues, statistical models

1. INTRODUCTION

The principles embedded in the circular economy are now emphasized in almost all manufacturing processes and product design. This has introduced several innovative concepts i.e. the bioeconomy, the bio-based society and the green economy that are now changing the strategic planning of many industrial companies [16].

The woodworking and furniture industries represent a sustainable, innovative and environmental economic sector, using a natural and renewable raw material and thus play a vital role in the development of green economy. Nowadays these wood-based industries, including the fibreboard sector, are facing an increased competition for wood resources from the renewable energy sector, due to the current legislative measures for promoting the use of wood for producing bioenergy to meet the respective renewable energy targets and by the development of innovative bio-based products [14]. Maximization of resource efficiency is a key objective to implement a circular economy and to face the challenges of increased demand for wood and wood-based products. To meet these demands sustainably requires action in a variety of areas, from the sustainable management of forests, to the more resource efficient use of wood in society. One of the leading principles is the so-called cascading use of wood resources: *"the efficient utilisation of resources by using residues and recycled materials for material use to extend total biomass availability within a given system"* [21].

The wood-based industries produce significant amounts of waste and residues. According to some authors [13] 26 million tonnes of post-consumer wood (wood products that are disposed at the end of their life cycle, e.g. wooden furniture, window frames and wood-based panels, packaging, doors, windows, various construction materials, etc.) was generated in Europe in 2010. Taking into account these figures it is

*Corresponding authour
Email: p.antov@gmail.com

European Mechanical Science, December 2018; 2(4): 140-145
doi: https://doi.org/10.26701/ems.443891
Received: July 13, 2018
Accepted: September 6, 2018

important to create different applications for the previous waste and residue materials while considering environmental and economic factors. Large quantities of wood wastes are also produced in the course of primary and secondary wood processing, including bark, sawmill shavings, slabs, off-cuts, rejects, wood chips and saw dust. These types of waste, sometimes called wood processing residues, are produced at industrial facilities and are easily collectable and reusable as feedstock for wood-based composite industry [7; 17; 20]. The total amount of wood processing residues in the EU28 was 178.7 Mm^3 in 2010, of which 82.3 Mm^3 were sawmill residues [21]. These residues represent an untreated and clean wood resource that can be used materially in the pulp and panel industry. The industrial reuse of wood resources will contribute greatly to the supply of raw material and will enhance the competitiveness of wood-based composite materials.

Fibreboards are a composite wood-based material with a dispersed phase of wood fibres and a composite matrix phase formed by the adhesion and cohesion bonds of the panels [1; 3].

Fibreboard production ranks second of all wood-based composites worldwide, outpaced only by the production of plywood and glued-laminated timber. The growth in the production of fibreboards for the period 2011 - 2015 was 45%, due mainly to the increased production of MDF panels, which accounted for 80% of the total production of fibreboards [30].

The defibraiton (disintegration of wood to free fibres) is one of the most energy-intensive processes in the production of this type of wood-based panels and has an important role in forming the final product costs [6; 9; 15]. Therefore, the design of exploitation properties of panels can be effectively performed by regulating the parameter values of the wood fibre mass incoming to the upper flow [8; 19]. When determining the raw material characteristics both the impact on the exploitation properties and production costs should be taken into consideration [12]. The reduction of product costs can be achieved by including wood industry residues in the composition of panels which do not need to go through the defibration process. The wood shavings, resulting from the primary and secondary wood processing with a bandsaw, represent a typical raw material for that purpose [2].

At present this type of wood processing waste and residues is mainly used in the production of wood pellets [4] and briquettes [11;18], as well as in the wood chemical industry for production of bioethanol [10]. It should be noted that the possibilities for utilization of wood shavings in one of the fastest-growing industries, namely the production of MDF panels, has not been sufficiently studied yet.

The adhesion bonds are of great importance in the production of fibreboards by dry processing method [5; 8]. The active area of contact between the fibres is reduced by including wood shavings in the composition of fibreboards, which can be compensated to some extent by increasing the bonding agent content.

The use of soft wood from deciduous tree species is recommended in the production of panels by dry processing method. The most widely used bonding agent is the urea-formaldehyde resin [5].

The present research is aimed at studying the possibilities of replacing a part of the wood fibre mass in the composition of combined medium density fibreboards (MDF) manufactured from poplar (*Populus alba* L.) with coniferous sawmill residues (shavings) from Scots pine (*Pinus sylvestris* L.) and the respective influence on the exploitation properties of the panels.

2. MATERIALS AND METHODS

The combined medium density fibreboards (MDF) were produced in laboratory conditions from wood fibre mass and coniferous sawmill residues (shavings). The wood fibre mass was obtained in factory conditions according to the Asplund method by using the *Defibrator* L-46 equipment. The wood fibre mass had a pulp freeness of 11° ShR and a bulk density of 29 $kg.m^{-3}$.

The coniferous wood shavings had a bulk density of 145 $kg.m^{-3}$. The fractional composition was as follows: fraction over 2.0 – 1.24%; fraction 2.0/1.0 – 25.71%; fraction 1.0/0.8 – 6.67%; fraction 0.8/0.5 – 34.2%; fraction 0.5/0.315 – 19.0%; fraction 0.315/0.2 – 9.25%; saw dust – 3.94%.

The wood shavings and fibres were dried to the uniform moisture content of 6%.

The studies on the influence of the composition on the exploitation properties of combined fibreboards manufactured with coniferous wood shavings were implemented by applying the simplex grid experimental plans with a two-fold constraint of the factors using the McLean and Anderson method [22]. The experimental matrix is presented in Table 1.

Table 1. Matrix of the experiments

№	Wood shavings content X_1	Content of urea-formaldehyde resin X_2	Content of fibres in absolute dry state X_3
1.	0.4	0.14	0.46
2.	0	0.08	0.92
3.	0.4	0.08	0.52
4.	0	0.14	0.86
5.	0.2	0.11	0.69
6.	0	0.11	0.89
7.	0.2	0.14	0.66
8.	0.2	0.08	0.72

The area of factor variation, corresponding to the above matrix, is presented on Fig. 1.

The panels were manufactured with a density of 720 $kg.m^{-3}$. The content of coniferous wood shavings was altered from 0 to 40%. The content of urea-formaldehyde resin was altered

Table 2. Results for the exploitation properties of combined fibreboards

№	Content of wood shavings X_1	Content of urea-formaldehyde resin X_2	Content of fibres in absolute dry state X_3	Bending strength f_m, N.mm^{-2}	Internal bond strength f_t, N.mm^{-2}	Swelling in thickness G_t, %	Water absorption A, %
1.	0.4	0.14	0.46	16.93	0.37	22.68	84.77
2.	0	0.08	0.92	21.55	0.21	25.87	60.26
3.	0.4	0.08	0.52	14.15	0.26	25.84	100.03
4.	0	0.14	0.86	24.22	0.32	19.49	50.73
5.	0.2	0.11	0.69	20.43	0.25	26.28	79.81
6.	0	0.11	0.89	25.35	0.38	19.74	37.37
7.	0.2	0.14	0.66	19.68	0.40	21.56	58.83
8.	0.2	0.08	0.72	17.01	0.23	28.07	101.20

Table 3. Regression models for determining the influence of coniferous wood shavings and urea-formaldehyde resin on the exploitation properties of combined fibreboards

Property	Bending strength f_m, N.mm^{-2}	Internal bond strength f_t, N/mm^{-2}	Swelling in thickness Gt, %	Water absorption A, %
Coefficient B_1	-48.729	0.595	–	82.098
Coefficient B_2	-3548.362	–	52.246	-242.394
Coefficient B_3	-31.044	–	36.146	85.524
Coefficient B_{12}	4705.522	–	–	–
Coefficient B_{13}	–	-0.465	50.000	226.065
Coefficient B_{23}	4572.727	3.206	-146.805	–
Coefficient B_{123}	-320.826	–	–	–
Determination coefficient R^2	0.985	0.610	0.861	0.865
Calculated value of the Fisher criterion F_{calc}	28.012	6.791	9.010	8.497
Critical value of the Fisher criterion F_{cr}	19.296	5.786	6.591	6.591

from 8 to 14% in order to compensate the negative impact of the inclusion of coniferous wood shavings in the composition of the manufactured MDF panels.

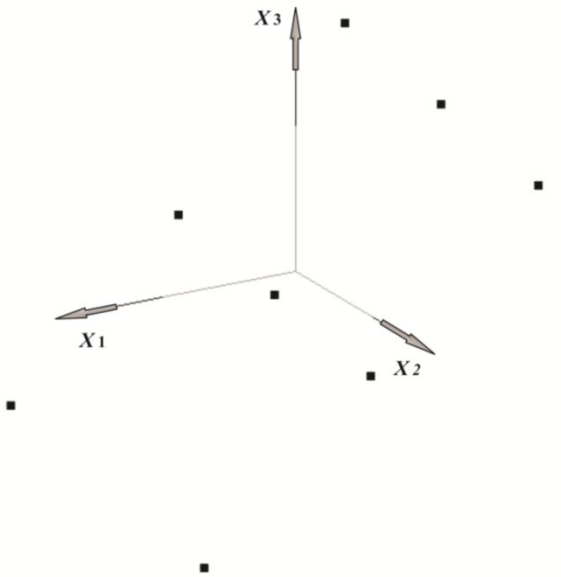

Fig. 1 Area of factor variation applying two-fold factor constraints for studying the influence of composition on the exploitation properties of combined fibreboards manufactured with coniferous wood shavings

The paraffin content was 1% of the absolutely dry wood. The additives were added for a period of 50 s by using a laboratory mixer at the speed of 850 min^{-1}. The pressing was performed on a laboratory press PMS CT 100, Italy. The hot pressing factor was 30 s.mm^{-1} of the panel thickness. The panels were manufactured with a thickness of 8 mm. The pressing temperature was 200° C. The hot pressing regime was as follows: I stage - pressure P = 4 MPa (15% of the whole cycle); II stage - pressure P = 2.0 MPa (15% of the whole cycle); III stage - pressure P = 0.8 MPa (50% of the whole cycle); IV stage - pressure P = 1.5 MPa (20% of the whole cycle).

The combined fibreboards were manufactured in laboratory conditions within the specified constraints. The properties of the panels were determined in accordance with the requirements of the applicable European standards in the respective field [23; 24; 25; 26; 27; 28]. The internal bond strength is determined to trace the bonding quality between the fibrous elements and between the fiber elements and the wood shavings.

The data was processed using specialized software (QstatLab) and stepwise regression at 1000 interactions was applied for determining the optimal values of the panel components.

3. RESULTS AND DISCUSSION

The summarized results for the exploitation properties of combined fibreboards with variation of the values (levels) of the coniferous wood shavings and urea-formaldehyde resin in accordance with the adopted experimental matrix are presented in Table 2.

The determination coefficient is used as a measure for determination of the approximation. The values of the regression coefficients, determination coefficient, calculated (F_{calc}) and critical (F_{cr}) value of the Fisher criterion, showing the regression models about the influence of the composition on the different exploitation properties of combined fibreboards, are presented in Table 3.

3.1 Analysis of the obtained experimental results for the bending strength of the panels

The influence of coniferous wood shavings and urea-formaldehyde resin on the exploitation properties of combined fibreboards manufactured of poplar and coniferous wood shavings is presented on Figure 2. By increasing the percentage of coniferous wood shavings up to 40% and reducing the content of urea-formaldehyde resin from 14 to 8%, a decrease of the bending strength values of the combined fibreboards is determined – from 25.3 to 14.2 N.mm^{-2}, i.e. as the result of the content variation of the boards there is a significant, more than 1.8 times, change in bending strength of the panels.

The optimal (maximum) value of the bending strength with a planned constraint of 23 N.mm^{-2} [29] for the value of the property which corresponds to the standard requirements for MDF panels with a predetermined board thickness is presented on the figure. The maximum value is reported at 11.59% urea-formaldehyde content, 0% wood shavings content and 88.38% content of poplar wood fibres. In order to achieve the requirements for the bending strength of fibreboards, the content of coniferous wood shavings can be increased up to 26% while the urea-formaldehyde content should be above 12%. When the binder content is 8%, the requirements for the bending strength of the panels could be achieved at the maximum permissible content of wood shavings up to 5%.

If the wood shavings content is increased above 10%, a significant deterioration of the bending strength values is observed which should be compensated by an increased binder content.

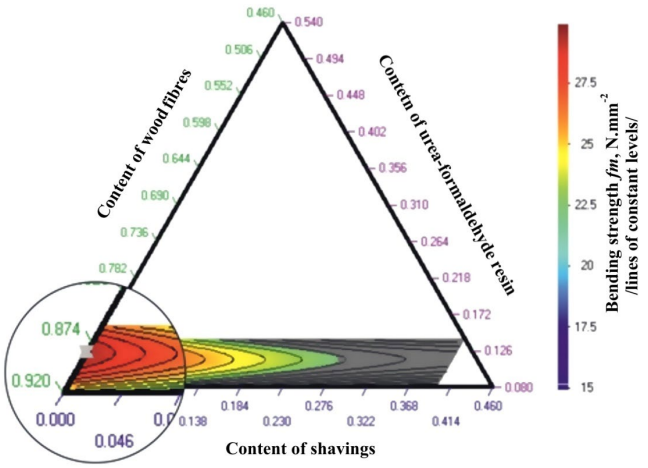

Fig. 2 "Composition-property" diagram for the bending strength of combined fibreboards manufactured with coniferous wood shavings

3.2 Analysis of the obtained experimental results for the internal bond strength of the panels

The graphical interpretation of the results for the influence of the composition on the internal bond strength of combined fibreboards manufactured of poplar wood and coniferous wood shavings is presented on Figure 3. The rage of variation of the examined property at the different panel compositions is from 0.21 to 0.40 N.mm^{-2}, i.e. the internal bond strength is decreased 1.9 times. The optimal (maximum) value of the internal bond strength of the manufactured combined fibreboards is also presented on the figure. The maximum value is determined at 14% content of urea-formaldehyde resin and without wood shavings in the composition of the panels. The greatest gradient of the property decrease is determined when increasing the wood shavings content above 10% and reducing the urea-formaldehyde content below 12%, respectively (transition to the orange zone of the graph).

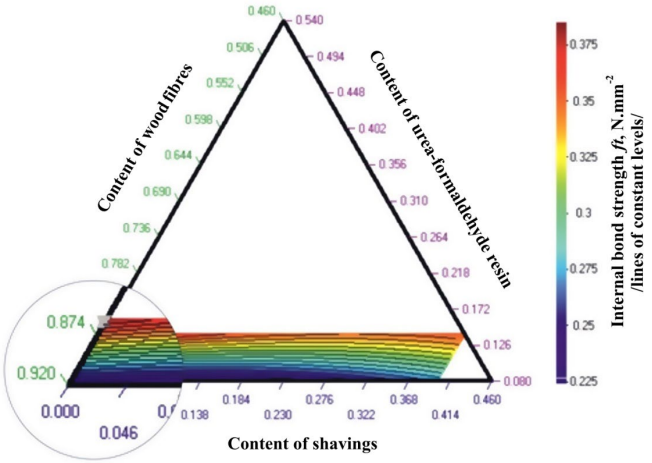

Fig. 3 "Composition-property" diagram for the internal bond strength of the combined fibreboards manufactured with coniferous wood shavings

3.3 Analysis of the obtained experimental results for the swelling in thickness and water absorption of the panels

The graphical interpretation of the dependence of the swelling in thickness of combined fibreboards manufactured of poplar wood and coniferous wood shavings is presented on Figure 4 by the "composition-property" diagram. The swelling in thickness of the panels varies from 19.5 to 28% within the studied range of factor variation, i.e. the swelling in thickness of the panels deteriorates 1.4 times by the increased content of coniferous wood shavings. The minimum value of the examined property is determined at 14% binder content and without coniferous wood shavings.

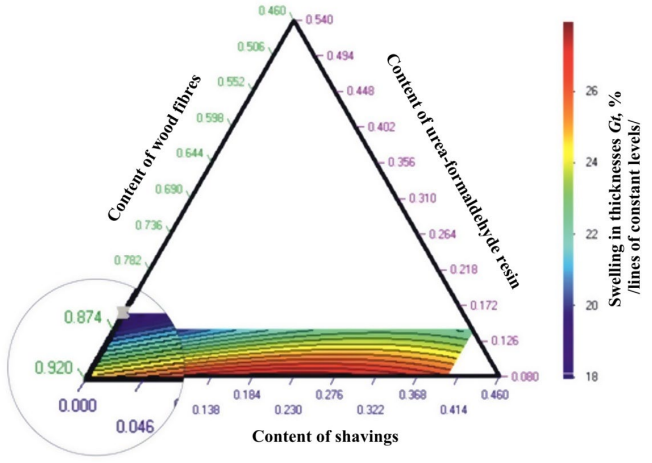

Fig. 4 "Composition-property" diagram for the swelling in thickness of the combined fibreboards manufactured with coniferous wood shavings

Upon analysis of the regression model and the graph, a distinct deterioration (increase) of the studied property is observed with the increase of wood shavings content above 10% and reduction of the bonding agent content below 12% (transition from the dark to light blue area of the graph).

The graphical representation of the influence of the panel composition on the water absorption of the panels is shown on Figure 5.

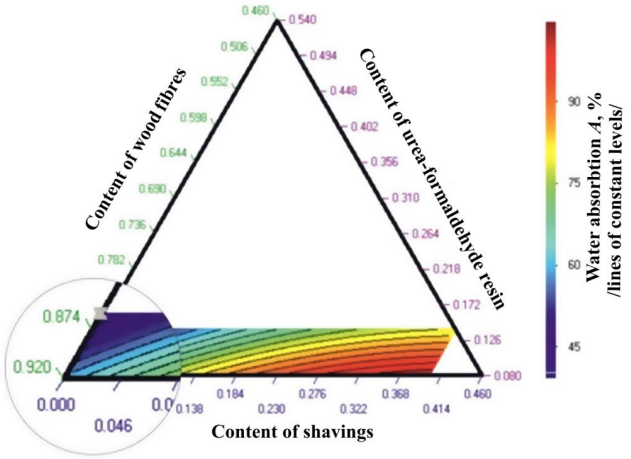

Fig.5 Composition-property" diagram for the water absorption of the combined fibreboards manufactured with coniferous wood shavings

The water absorption of the panels varies within the range from 101.2 to 37.4 %. The most significant deterioration of all studied exploitation properties is determined for the water absorption (2.7 times) as the result of the addition of coniferous wood shavings and reduction of the binder content.

The optimal value of the property is obtained at 14% content of urea-formaldehyde resin without the inclusion of wood shavings.

Regarding the water absorption of the panels two main dividing values of the wood shavings content are determined, after which a significant deterioration or increase of the values of the studied property is reported. The first significant increase of the gradient is observed after exceeding the value of 10% wood shavings content and the second one – above 26% wood shavings content. As for the binder content a significant deterioration of the values of the water absorption is determined at reduction below 12%.

4. CONCLUSIONS

After conducting the present research and analysing the obtained experimental results for the influence of the composition on the exploitation properties of combined fibreboards manufactured of poplar wood and coniferous wood shavings, the following main conclusions can be drawn:

1) A significant deterioration of the studied exploitation properties of the panels is determined after including coniferous wood shavings in the composition of poplar fibreboards due to the decreased area of active contact between the fibrous elements;

2) As a result of the variation of coniferous wood shavings from 0 to 40% and reduction of the urea-formaldehyde content from 14% to 8%, the decrease in bending strength and internal bond strength of the panels is almost twice;

3) The negative impact on the swelling in thickness of the panels, resulting from the increased coniferous wood shavings content and reduced urea-formaldehyde content, is 1.4 times; the most significant influence of the composition of the panels is determined for their water absorption where a deterioration of 2.7 times is reported;

4) Regarding the influence on the exploitation properties of combined poplar fibreboards manufactured with coniferous wood shavings, the percentage contribution to the latter should be no more than 26%; after exceeding the 10% wood shavings content the minimum urea-formaldehyde content should be 12%;

5) When the urea-formaldehyde content in the composition of the combined fibreboards is up to 10%, the maximum content of coniferous wood shavings should not exceed 5%.

ACKNOWLEDGEMENTS

This work was supported by the project BG-05M2OP001-2.009-0034 "Support for the Development of Scientific Capacity in the University of Forestry", funded by the Operational Program "Science and Education for Smart Growth" (2014-2020) and implemented by the University of Forestry, Sofia, Bulgaria.

REFERENCES

[1] Ayrilmys N, Yurttas E, (2017) Effect of core layer fiber size and face to core layer ratio on properties of three layered fiberboard. BioResources 12(4):7964-7974.

[2] Bello RS (2017) Characterization of Sawdust Produced from Circular, Chain and Band Sawing Machines. Bioprocess Engineering. Vol. 1, No. 1:21-29.

[3] Benthien JT, Bahnisch C, Heldner S, Ohlmeyer M (2014) Effect of fiber size distribution on medium-density fiberboard properties caused by varied steaming time and temperature of defibration process. Wood and Fiber Science 46(2):175-185.

[4] Bergström D, Israelson S, Öhman M, Dahlquist SA, Gref R, Boman C (2008) Effects of raw material particle size distribution on the characteristics of Scots pine sawdust fuel pellets. Fuel Processing Technology 6.

[5] Thoemen H, Irle M, Sernek M (2010) Wood-Based Panels an Introduction for Specialists. Brunel University Press.

[6] Hellström LM, Carlberg T, Engstrand P, Gradin PA, Gregersen ØW (2012) Evaluation of collimated chipping technology for reducing energy consumption in mechanical pulping. Journal of Science & Technology for Forest Products and Processes 2(3).

[7] Hillring B, Canals G, Olsson O (2007) Market for recovered wood in Europe - an overview. In: Gallis Ch (ed) Management of recovered wood. University Studio Press, Thessaloniki.

[8] Htun M, Salmén L (1996) The importance of understanding the physical and chemical properties of wood to achieve energy efficiency in mechanical pulping. Wochenbl. Papierfabrik 124: 232-235.

[9] Hua J, Chen G, Xu D, Shi SQ (2012) Impact of termomechanical refining conditions on fiber quality and energy consummation by mill trial. BioResources 7(2):1919-1930.

[10] Irawati D, The utilization of sawdust for ethanol production. http://repository.ipb.ac.id/handle/ doi: 123456789/9013. (accessed 17 May 2014).

[11] Kupolati WK, Grassi St, Frattari A (2012) Environmental Greening through Utilization of Sawdust for Production of Bricks. OIDA International Journal of Sustainable Development, Vol. 4, No. 12:63-78.

[12] Li J, Pang S, Scharpf EW (2012) Modeling of thermal energy demand in MDF production. Forest Prod. J. 57(9):97-104.

[13] Mantau, U. (2012) Wood Flows in Europe. Commissioned by CEPI: Confederation of European Paper Industries, and CEI-Bois: European Confederation of Woodworking Industries.

[14] Mantau U. (2010) Wood resource balance results - is there enough wood for Europe? In: Mantau U et al (ed) Euwood - Real potential for changes in growth and use of EU forests. Final report, Hamburg:19–34.

[15] Martínez A, Huber CD, Pinkl S, Mahrdt E, Teischinger A, Müller U (2017) Dynamic Compression: A Novel Technique to Reduce Energy Consumption during Wood Fiber Production. BioResources 12(4):7376-7394.

[16] McCormick K, Kautto N (2013) The bioeconomy in Europe: an overview. Sustainability 5:2589–2608.

[17] Merl AD, Humar M, Okstad T, Picardo V, Ribeiro A, Steierer F (2007) Amounts of recovered wood in COST E31 countries and Europe. In: Gallis Ch (ed) Management of recovered wood. University Studio Press, Thessaloniki:79–116.

[18] Pushpa J, Pramod Y (2012) Briqueting of saw dust. Applied Mechanics and Materials Vols. 110-116:1758-1761.

[19] Shi JL,. Zhang SY, Riedl B (2006) Multivariate modeling of MDF panel properties in relation to wood fiber characteristics, Holzforschung. 60(3):285-293.

[20] Vefago LHM, Avellaneda J (2013) Recycling concepts and the index of recyclability for building materials. Resour Conserv Recycl 72:127–135.

[21] Vis M, Mantau U, Allen B (Eds.) (2016) Study on the optimised cascading use of wood. No 394/PP/ENT/RCH/14/7689. Final report. Brussels:337.

[22] Wang Z, Ye W, Chu I, Ong ShP (2016) Elucidating Structure–Composition–Property Relationships of the β-SiAlON:Eu2+ Phosphor. Chemistry of Materials.

[23] EN 310: 1993 "Wood-based panels - Determination of modulus of elasticity in bending and of bending strength".

[24] EN 316:2009 "Wood fibreboards - Definition, classification and symbols".

[25] EN 317:1993 "Particleboards and fibreboards - Determination of swelling in thickness after immersion in water".

[26] EN 319:1993 "Particleboards and fibreboards - Determination of tensile strength perpendicular to the plane of the board".

[27] EN 322:1993 "Wood-based panels - Determination of moisture content".

[28] EN 323:1993 "Wood-based panels - Determination of density".

[29] EN 622-5:2009 "Fibreboards - Specifications - Part 5: Requirements for dry process boards (MDF)".

[30] Global production and trade of forest products in 2016 http://www.fao.org/forestry/statistics (accessed 05 January 2018).

EUROPEAN MECHANICAL SCIENCE

Instructions for authors

All manuscripts must be in English. Pages should be numbered sequentially. The manuscript should be composed in accordance with the Article Template given above. The maximum length of contributions is 10 pages. For full instructions see the Information for Authors section on the journal's website:

http://dergipark.gov.tr/ems/page/2805

FORMAT OF THE MANUSCRIPT

The manuscript should be composed in accordance with the Article Template.

The manuscript should be written in the following format:

- A Title that adequately describes the content of the manuscript.

- A list of Authors and their affiliations.

- An Abstract that should not exceed 850 words. The Abstract should state the principal objectives and the scope of the investigation, as well as the methodology employed. It should summarize the results and state the principal conclusions.

- 4-6 significant key words should follow the abstract to aid indexing.

- An Introduction that should provide a review of recent literature and sufficient background information to allow the results of the article to be understood and evaluated.

- An Experimental section that should provide details of the experimental set-up and the methods used to obtain the results.

- A Results section that should clearly and concisely present the data, using figures and tables where appropriate.

- A Discussion section that should describe the relationships and generalizations shown by the results and discuss the significance of the results, making comparisons with previously published work. (It may be appropriate to combine the Results and Discussion sections into a single section to improve clarity.)

- A Conclusions section that should present one or more conclusions drawn from the results and subsequent discussion and should not duplicate the Abstract.

- Acknowledgement (optional) of collaboration or preparation assistance may be included. Please note the source of funding for the research.

- References must be cited consecutively in the text using square brackets [1] and collected together in a reference list at the end of the manuscript.

FIGURES

Figures (figures, graphs, illustrations digital images, photographs) must be cited in consecutive numerical order in the text and referred to in both the text and the captions as Fig. 1, Fig. 2, etc. Figures should be prepared without borders and on white grounding and should be sent separately in their original formats. If a figure is composed of several parts, please mark each part with a), b), c), etc. and provide an explanation for each part in Figure caption. The caption should be self-explanatory. Letters and numbers should be readable (Arial or Times New Roman, min 6 pt with equal sizes and fonts in all figures).

Graphics (submitted as supplementary files) may be exported in resolution good enough for printing (min. 300 dpi) in any common format, e.g. TIFF, BMP, GIF or JPG, PDF and should be named Fig1.jpg, Fig2.tif, etc. However, graphs and line drawings should be prepared as vector images, e.g. CDR, AI.

Multi-curve graphs should have individual curves marked with a symbol or otherwise provide distinguishing differences using, for example, different thicknesses or dashing.

TABLES

Tables should carry separate titles and must be numbered in consecutive numerical order in the text and referred to in both the text and the captions as Table 1, Table 2, etc. In addition to the physical quantities, such as t (in italics), the units (normal text) should be added in square brackets. Tables should not duplicate data found elsewhere in the manuscript. Tables should be prepared using a table editor and not inserted as a graphic.

RERERENCES

A reference list must be included using the following information as a guide. Only cited text references are to be included. Each reference is to be referred to in the text by a number enclosed in a square bracket (i.e. [3] or [2] to [4] for more references; do not combine more than 3 references, explain each).

References must be numbered and ordered according to where they are first mentioned in the paper, not alphabetically. All references must be complete and accurate. Please add DOI code when available. Examples follow.

Journal Papers:

Surname 1, Initials, Surname 2, Initials (year). Title. Journal, volume, number, pages, DOI code.

[1] Calikoz, R., Ozcanli, B., Serin, F., (2017). Simulating nonlinear materials under vertical forces by using intelligent . European Mechanical Science, 57(8): 531-538, DOI:10.5545/ems.2017.013.

Journal titles should not be abbreviated. Note that journal title is set in italics.

Books: Surname 1, Initials, Surname 2, Initials (year). Title. Publisher, place of publication.

[2] Ozgur, M.P. (2012). Fundamentals of Mechanical Engineering. Gunlubey, Ankara.

Chapters in Books:

Surname 1, Initials, Surname 2, Initials (year). Chapter title. Editor(s) of book, book title. Publisher, place of publication, pages.

[3] Akarca, G., Gelidor, M. (2016). Mechanical robotic systems. Calikca, V., Kurbetoglu, A., Merdan, M. (Eds.), Cutting Edge Robotics. Literatur Bergli, Mammendorf, 553-576.

Proceedings Papers:

Surname 1, Initials, Surname 2, Initials (year). Paper title. Proceedings title, pages.

[4] Seferci, N., Malikoglu, S., Tosun, N. (2009). Applied mechanic in process industry. IMSEC 2016 Conference Proceedings, 422-427.